Engineering Fracture Mechanics 313 (2025) 110662

Contents lists available at ScienceDirect

Engineering Fracture Mechanics

journal homepage: www.elsevier.com/locate/engfracmech

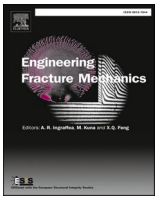

An innovative wide-ranging analytical approach for modelling the bond behaviour of frp-to-substrate joints with an elastic end anchorage

Hugo C. Biscaia [a,b,*], Jian-Guo Dai [c]

[a] UNIDEMI, Department of Mechanical and Industrial Engineering, NOVA School of Science and Technology, 2829-516 Caparica, Portugal
[b] Laboratório Associado de Sistemas Inteligentes, LASI, 4800-058 Guimarães, Portugal
[c] Department of Architecture and Civil Engineering, City University of Hong Kong, Hong Kong, China

ARTICLE INFO

Keywords:
FRP composites
Analytical approach
Debonding
Anchorages
Single-lap shear test

ABSTRACT

Fibre-reinforced polymers (FRP) are often externally bonded (EB) to concrete, steel or timber structures for structural strengthening purposes. In the EB reinforcement system, the bond between materials is critical for the success of such a bonding system. However, the system is prone to debond at an FRP strain level much lower than its rupture value. For this reason, it is often necessary to use end anchorages in FRP-strengthened beams to delay or avoid this premature debonding of FRP from the beams. To better understand the debonding process of mechanically anchored FRP-to-substrate joints, the present work proposes a new analytical approach that considers an elastic end anchorage, which can simulate, through a spring, the slips developed in an end anchorage such as an FRP U-wrap jacket, FRP spike anchor, steel plate anchorage, among others. This new approach can also simulate the bond performance of FRP-to-substrate joints with no end anchorages by assuming that the stiffness of the end anchorage is zero. Expressions for defining the load-slip curves, FRP strains, interfacial slips, and bond stresses developed throughout the bonded length are derived and validated against the results from the Finite Element Analysis (FEA). In the end, the model was used to simulate several experimental tests on mechanically anchored FRP-to-substrate joints available in the literature. Despite its simplicity, the proposed analytical approach covers wider situations that no other known similar approach can deal with.

1. Introduction

The need to repair or strengthen existing damaged structures with fibre reinforcement polymers (FRP) through the externally bonded reinforcement (EBR) system has grown in the past few decades. However, by itself, the EBR system has been revealed not to be efficient enough since its failure often occurs by the FRP debonding when the FRP strain is well below its rupture value. Thus, to delay or even prevent the premature debonding of the FRP composite from the substrate, several authors have developed and experimentally or numerically tested different anchorage systems to be added to the EBR system [1–10]. Due to such a variety of anchorage solutions, the prediction of the bond performance of each anchored FRP-to-substrate joint is always restrictive since it is applicable only to a

* Corresponding author at: UNIDEMI, Department of Mechanical and Industrial Engineering, NOVA School of Science and Technology, 2829-516 Caparica, Portugal.
E-mail address: hb@fct.unl.pt (H.C. Biscaia).

https://doi.org/10.1016/j.engfracmech.2024.110662
Received 27 August 2024; Received in revised form 15 October 2024; Accepted 14 November 2024
Available online 17 November 2024

Nomenclature

A_r	is the cross-sectional area of the reinforcement
A_s	is the cross-sectional area of the substrate
B	is the stiffness index of the interface
b_r	is the width of the reinforcement
C_1	is the first constant obtained from integration
C_2	is the second constant obtained from integration
d^{FEM}	is the data calculated from the FEM
d^{PAA}	is the data obtained from the proposed analytical approach
E_r	is the elastic modulus of the reinforcement
ε_r	is the strain developed in the reinforcement
ε_{r0}	is the strain developed at the reinforcement-free end
$\varepsilon_{r\max}$	is the maximum strain developed in the reinforcement
E_s	is the elastic modulus of the substrate
F_0	load transmitted to the anchorage system
G_F	is the mode II fracture energy
λ	is a constant parameter
k	stiffness (or slope) of the load-slip curve of the anchorage system
L_b	is the bonded length
n	is the number of measurements carried out during the simulations of the debonding process
r	is the ratio between the axial stiffness of the reinforcement and the axial stiffness of the substrate
s	is the interfacial slip
s_0	slip at the mechanically anchored fibre-reinforced polymer
s_{Lb}	is the slip at the reinforcement-loaded end
$s_{\max}$	is the interfacial slip at maximum bond stress
τ_b	is the bond stress
$\tau_{b\max}$	is the maximum bond stress predicted in the bond-slip relationship
t_r	is the thickness of the reinforcement
x	is the longitudinal coordinate parallel with the bond line of the joint

limited number of specimens or a specific anchorage type.

Anchorages are usually made of Carbon FRP (CFRP) sheets or steel or if the substrate has a low tensile strength such as concrete, the concrete surface can be replaced by resin. For the former case, a common and simple anchorage system may consists of increasing the width of the FRP composite by wrapping the end of the FRP with CFRP sheets. Considering that the maximum load transmitted to the CFRP composite is directly proportional to the FRP width [11–17], the U-wrap jacketing seems to be a rational solution to anchor the FRP-to-substrate bonded joints. However, to alleviate the concentrated shear stresses at the interface due to the discontinuity between the anchorage and the EBR system, a smooth transition in that region should be adopted [7]. However, the U-anchoarage can not stop the development of slips of FRP and the failure canstill be due to excessive slip of the EB-FRPrather than the FRP rupture [18]. To improve the stress transfer between adherends, the use of CFRP spike anchors is another anchorage technique. This anchorage technique consists of introducing a hold into the substrate, and embedding a CFRP spike anchor. The hole is filled with resin and the head of the spike anchor is bonded to the EB-FRP sheet. Since it is necessary to drill holes in the substrate, the use of such anchorage technique is not advisable for steel structures. The main issue associated with such CFRP spike anchors is the magnitude of normal/shear stresses induced by FRP sheet on the spike anchor during the debonding process. So far, the number of CFRP spike anchors or the space between them is a topic not properly answered yet despite the extensive efforts devoted to this topic, e.g. [19–22].

Within the context of CFRP anchorages, a quite promising technique that can avoid the premature debonding of FRP composite is the Continuous Reinforcement Embedded at Ends (CREatE) [23–25] (see Fig. 1). This anchorage technique aims to anchor both ends of FRP strips using an EBR or a near-surface mounted (NSM) FRP or steel bar (or rod) into the end of the substrate. For instance, in the case of a simple supported reinforced concrete (RC) beam, two holes should be drilled close to the supports (one hole per FRP or steel end) and both ends of FRP strips were anchored into the holes through an embeddement of the FRP or steel bars (or rods) [24]. This

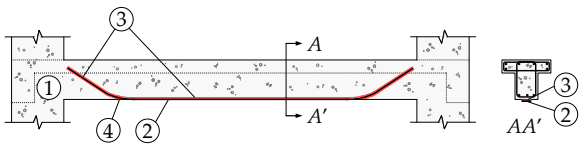

Key: 1 – RC beam; 2 – FRP sheet/strip or steel bar/rod; 3 – Adhesive; 4 – Transition curve.

Fig. 1. RC beam flexurally-strengthened according to the Continuous Reinforcement Embedded at Ends (CREatE) technique.

innovative anchorage technique showed not only the improvement of the flexural behaviour of RC beams but also decreased the strains in the stirrups, suggesting that the RC beam's shear strengthening can be simultaneously achieved [24]. Like the CFRP spike anchors, this anchorage system is more appropriate for concrete, timber or brick structures than steel structures. In addition, the use of FRP strips or even stainless steel within this anchorage system is preferred over FRP sheets.

The use of a steel plate is another popular choice for the end anchorage system among researchers, e.g. [26–32]. In this anchorage system, the steel plate is externally pressured against the FRP composite and fixed through steel bolts to the substrate. By pressuring the FRP composite against the substrate, the local bond performance is enhanced, i.e., the maximum bond stress increases. After the FRP debonds, the friction between the FRP and the substrate contributes to the increase of the load transmitted to the FRP composite

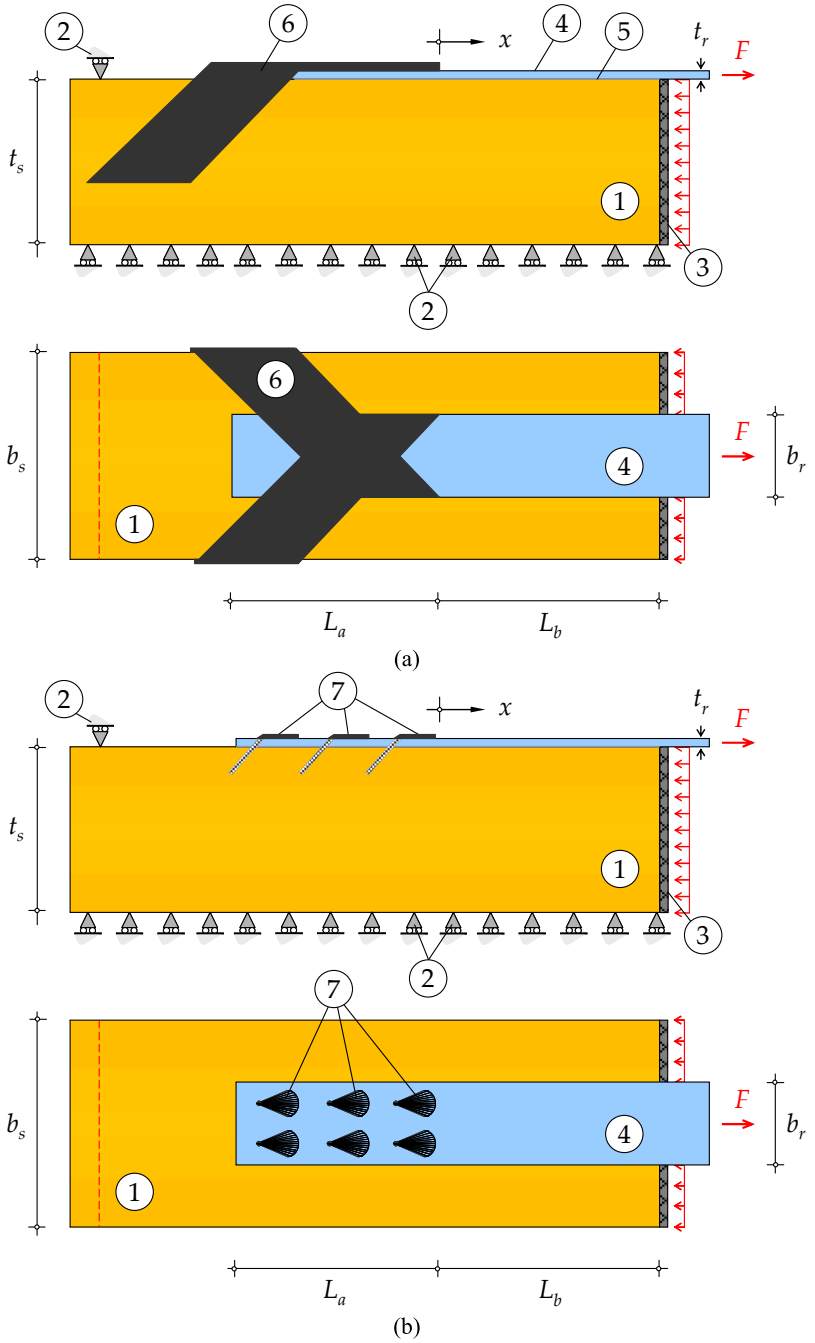

Key: 1 – Substrate; 2 – Roller support; 3 – Steel reaction plate; 4 – FRP sheet/strip; 5 – Adhesive; 6 – CFRP U-wrap jacket; 7 – CFRP spike anchor.

Fig. 2. FRP-to-substrate bonded joint with an FRP end anchorage: (a) U-wrap jacket; and (b) spike anchor.

[33–35]. Despite its efficiency, some issues also arise. For instance, if the steel plate is overpressured against the FRP composite, the fibres can be damaged or, if underpressured, the anchorage may allow the development of relevant slips that compromise the efficiency of the anchorage. It is noted that this end anchorage is fixed to the substrate through metallic fasteners and can be applied to any substrate material.

All these above-mentioned anchorage systems exhibit different bond performances [36,37]. However, the magnitude of slip of the EB-FRP composite under the anchorage is still most meaningful. Numerical strategies have been successfully used to describe the debonding process of anchored CFRP-to-substrate joints subjected to a mode II load, e.g. [9]. However, simple design-oriented approaches dealing with such anchored joints are scarce in the literature, and the existing ones usually consider the specific case of no slip in the end anchorage [30] or assume a simple piecewise bond-slip relationship for the whole joint [38]. For instance, Biscaia et al. [30] have proposed an analytical approach to predict the bond performance of an anchored FRP-to-substrate joint by using an exponential bond-slip relationship for the whole joint, which facilitates the analysis of the full debonding process of a perfectly anchored FRP-to-substrate joint, i.e., no slips are considered in the anchorage. This may not reflect the reality since the FRP composite may slip from the anchorage. Also, the analytical model is not applicable for a joint free of any anchorage system. Lu et al. [38] recently proposed an interesting analytical approach based on a triangular bond-slip relationship by considering that a U-wrap jacket is represented by a linear spring. The analytical approach fitted very well with the experiments, in which the joint had a bonded length longer than the effective bond length [39–41]. However, since the bond-slip relationship is a piecewise function, it requires several equations to describe the full debonding process of anchored CFRP-to-concrete, which makes its implementation difficult. They [38] only studied the case of end anchorages where the CFRP slips from the anchorage and in those cases, the load-slip curves showed a snap-back and a snap-through phenomenon. As the CFRP debonds from the substrate, the snap-back can be observed, and due to the influence of the spring, the loads increase linearly with the slip at the final stage, when the CFRP has fully debonded from the substrate.

It is essential to facilitate a better understanding of the general bond performance of EB-FRP systems (especially with an end-anchorage system) and provide engineers and practitioners with more straightforward and versatile approaches. The present work aims to present an innovative analytical approach to address such a need. This analytical approach can predict the load-slip curve, strains in the adherents and bond stress developed in the interface, and the full-range debonding process of FRP-to-substrate joints without an anchorage or with an elastic end-anchorage. The local bond-slip relationship for the unanchored FRP-to-substrate interface is approximated with a widely accepted exponential function [12]. To validate the proposed analytical approach, specimens with different design parameters were modelled with the Finite Element Method (FEM), and five other studies available in the literature were also simulated [27,29,37,38,42]. An effective (i.e., threshold) stiffness for the end anchorage was identified, i.e., a stiffness beyond which the debonded load can be increased due to the contribution of the anchorage. Despite its simplicity, the proposed design-oriented solutions for the prediction of the bond performance of a general FRP-to-substrate joint, i.e. with and without an end anchorage, provides a good option to be considered in the development of future international guidelines, and covers a wider range applications that exisintg analytical approach could not reach.

2. Proposed analytical approach

To facilitate the comprehension of the proposed analytical approach, the current section enframes all debonding problems into which the analytical approach falls. The limitations and initial assumptions on which the approach is based are pointed out and all the analytical derivations to obtain the load-slip curves, slip and bond stress distributions as well as the strains developed in the adherends are reported.

2.1. Problem description

The use of an end anchorage to delay or even prevent premature debonding of the EB-FRP composite from the substrate has become a common practice. Fig. 2 shows a couple of examples of these end anchorages. One consists of an FRP U-jacket anchor (see Fig. 2a) and the other consists of an FRP spike anchor (see Fig. 2b). In both cases, the anchorage load is denoted as F_0 whereas the load transmitted to the EB-FRP composite is denoted as F. It is assumed that the load-slip curve of the joint portion with an FRP U-jacket or with an FRP spike anchor is approximately linearly ascendent until the failure and, therefore, it can be replaced by a spring mounted at the free end (i.e., at the beginning of the loading stage) of EB-FRP [38]. Thus, the load-slip curve of such end anchorage can be defined as:

$$F_0 = k \cdot s_0 \tag{1}$$

where s_0 is the slip at the mechanically anchored FRP end; and k is the stiffness (or slope) of the load-slip curve of the anchorage system.

The bonded length of the anchorage is not reflected in Eq. (1) and the debonding is consistent with the single-lap shear tests where the bending of neither the FRP nor the substrate is considered, i.e., only axial deformation of the FRP and the substrate are assumed. In these conditions, the 2nd-order differential equation that governs the debonding problem is [11,38,43–47]:

$$\frac{d^2 s}{dx^2} - \lambda \cdot \tau_b = 0 \tag{2}$$

where τ_b is the bond stress developed within the interface between the FRP composite and the substrate; s is the relative displacement (or slip) between adherends; x is the longitudinal coordinate parallel with the bonded length of the joint; and λ is given by

$$\lambda = \frac{1}{E_r \cdot t_r} + \frac{b_r}{E_s \cdot A_s} \tag{3}$$

where E_r and E_s are the elastic moduli of the EB-FRP composite and substrate, respectively; t_r and b_r are, the thickness and width of the EB-FRP composite, respectively; and A_s is the cross-sectional area of the substrate.

The solution of Eq. (2) depends on the local bond behaviour of the joint, i.e., depends on τ_b. So, depending on the materials used as adherends [48], adhesive type [49–51] or stresses developed perpendicularly to the bonded area [33–35], the local bond behaviour is different and maybe mathematically defined by different expressions that correlate the local interfacial slips with the corresponding local bond stresses developed in the interface. This relationship is commonly denoted as a bond-slip relationship and several different expressions can be found in the literature [12,34,51–61]. To allow for an easier determination of the analytical solution for Eq. (2), the continuous exponential bond-slip relationship (instead of a segmental bilinear or a trilinear one) proposed by Dai et al. [12] is used and further details are reported in Subsection 2.3.

2.2. Initial assumptions

Before derivating the analytical expressions that intend to describe the full debonding process of end-anchored FRP-to-substrate joints, the following initial assumptions are enumerated:

(i) the thickness of the adherends remains unchanged during the full debonding process of the FRP-to-substrate joint with or without an end anchorage;
(ii) the adherend components (i.e., FRP and concrete/steel/timber or other structural material) have a linear elastic behaviour until the failure of the bonded joints;
(iii) during the debonding process, the peeling stresses can be ignored and only the deformations consistent with mode II are considered. That is, the FRP-to-substrate joints with or without an end anchorage are subjected to mode II loading;
(iv) the interface between FRP and the substrate (including the adhesive layer) can be replaced by a non-thickness cohesive zone model (CZM) whose behaviour, under Mode II loading, is described by a local bond-slip relationship [55,57,62–68]. In the present paper, an exponential bond-slip relationship is used to approximate such behaviour;
(v) the bond stresses across the width of the FRP composite is constant;
(vi) the U-jacket, spike anchor, steel plate or any other end anchorage has a linear load-slip behaviour, which can be modelled by a linear spring as shown in Fig. 3;
(vii) the FRP-to-substrate bonded joints without an end anchorage are modelled by assuming a marginal stiffness value for the above-mentioned spring to minimize its influence on the debonding process;
(viii) in the case, for instance, of a steel substrate, its yielding is not explicitly considered in the modelling. However, once the strains developed in the adherends are known, the analytical approach can predict the failure load corresponding to the yielding of the steel (i.e., the failure of the spring), the rupture of the FRP composite, or the debonding of the FRP composite from the substrate.

2.3. Exponential bond-slip relationship

As already mentioned, the exponential bond-slip relationship used in this work was originally proposed by Dai et al. [12] to describe the local bond behaviour between an FRP composite and a concrete substrate. However, it can also be used as an approximation to describe the debonding process of a general bonded joint. Its versatility for integration or derivation allows for the determination of analytical solutions of Eq. (2) [12,34]. This bond-slip relationship is characterized by an initial Elastic (E) stage, Softening (S) stage, and Debonding (D) stage (see Fig. 4). In the E stage, the bond stresses increase with the slips nonlinearly until a maximum

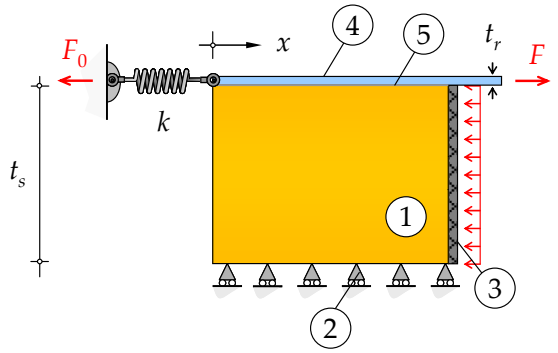

Key: 1 – Substrate; 2 – Roller support; 3 – Steel reaction plate; 4 – FRP strip; 5 – Adhesive.

Fig. 3. Idealized FRP-to-substrate bonded joint with an end anchorage simulated by a spring with a stiffness k_0.

bond stress ($\tau_{b\max}$) is reached. Then, the S stage corresponds to the bond stress decrease with the slip increase. This decrease is also nonlinear and, for infinite slip, it tends to zero bond stress. For small values of bond stresses, the bond stress transfer between adherends may be ignored and, therefore, a crack formation and development in the interface occurs, which corresponds to the D stage.

To obtain this exponential bond-slip relationship, it is needed first to approximate the experimental FRP strain (i.e., load)-slip curve to the following expression:

$$\varepsilon_r = \varepsilon_{r\max} \cdot \left(1 - e^{-B \cdot s}\right) \tag{4}$$

where $\varepsilon_{r\max}$ is the maximum strain developed in the FRP composite at the debonding initiation; and B is the stiffness index of the interface, which is used to fit Eq. (4) to the experimental data [12].

From an equilibrium point of view of the FRP composite, the following expression can be obtained:

$$\tau_b = E_r \cdot t_r \cdot \frac{d\varepsilon_r}{dx} = E_r \cdot t_r \cdot \frac{d\varepsilon_r}{ds} \cdot \frac{ds}{dx}. \tag{5}$$

Derivating Eq. (4) with respect to x and introducing it into Eq. (5), yields:

$$\tau_b = E_r \cdot t_r \cdot \varepsilon_{r\max}^2 \cdot B \cdot e^{-B \cdot s} \cdot \left(1 - e^{-B \cdot s}\right). \tag{6}$$

The integration of Eq. (6) with respect to s allows for the determination of the mode II fracture energy, i.e.,

$$G_F = \int_0^{\infty} \tau_b ds, \tag{7}$$

which leads to

$$G_F = \frac{E_r \cdot t_r \cdot \varepsilon_{r\max}^2}{2}. \tag{8}$$

Thus, the maximum strain developed in the FRP composite can be predicted according to

$$\varepsilon_{r\max} = \sqrt{\frac{2G_F}{E_r \cdot t_r}}. \tag{9}$$

Finally, by introducing Eq. (9) into Eq. (6), the exponential bond-slip relationship proposed by Dai et al. [12] can be obtained:

$$\tau_b = 2B \cdot G_F \cdot \left(e^{-B \cdot s} - e^{-2B \cdot s}\right). \tag{10}$$

Moreover, when the first derivative of Eq. (10) with respect to s is carried out and equating to zero, the slip corresponding to the maximum bond stress is

$$s_{\max} = \frac{\ln(2)}{B}, \tag{11}$$

which introduction into Eq. (10), allows for the determination of the maximum bond stress predicted in this bond-slip relationship as follows

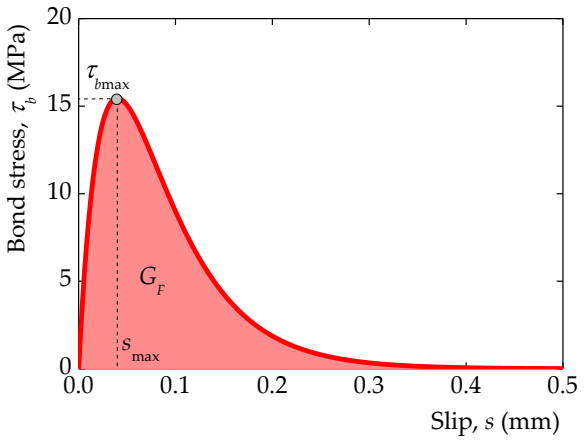

Fig. 4. Exponential bond-slip relationship proposed by Dai et al. [12].

$$\tau_{bmax} = \frac{B \cdot G_F}{2}. \tag{12}$$

2.4. Analytical solution of the governing equation

Once the mechanical properties of the materials, the geometry and dimensions of the bonded joint as well as the stiffness of the end anchorage are defined, Eq. (2) can be solved. Thus, the governing equation of the debonding process of the FRP-to-substrate is obtained by introducing the exponential bond-slip relationship defined in (10) in Eq. (2), which yields:

$$\frac{d^2s}{dx^2} - 2\lambda \cdot B \cdot G_F \cdot \left(e^{-B \cdot s} - e^{-2B \cdot s}\right) = 0. \tag{13}$$

Considering that

$$\frac{d^2s}{dx^2} = \frac{d}{dx}\left(\frac{ds}{dx}\right) = \frac{d}{ds}\left(\frac{ds}{dx}\right)\frac{ds}{dx} = \frac{1}{2} \cdot \frac{d}{ds}\left(\frac{ds}{dx}\right)^2, \tag{14}$$

Eq. (13) can be rewritten as

$$\left(\frac{ds}{dx}\right)^2 = \int 4\lambda \cdot B \cdot G_F \cdot \left(e^{-B \cdot s} - e^{-2B \cdot s}\right) ds. \tag{15}$$

Bearing in mind also that

$$2B \cdot \left(e^{-B \cdot s} - e^{-2B \cdot s}\right) = \frac{d}{ds}\left(1 - e^{-B \cdot s}\right)^2, \tag{16}$$

Eq. (15) can be rewritten, once again, as

$$\left(\frac{ds}{dx}\right)^2 = \int 2\lambda \cdot G_F \cdot \frac{d}{ds}\left(1 - e^{-B \cdot s}\right)^2 ds. \tag{17}$$

Integrating Eq. (17) yields:

$$\frac{ds}{dx} = \sqrt{2\lambda \cdot G_F \cdot \left(1 - e^{-B \cdot s}\right)^2 + C_1} \tag{18}$$

where C_1 is a constant to be found from the strain developed at the FRP composite free end (ε_{r0}), which can be obtained from the general expression proposed by the authors [51,69,70]:

$$\varepsilon_r = \frac{1}{1+r} \cdot \frac{ds}{dx} \tag{19}$$

where r is the ratio between the axial stiffness of the FRP composite and the axial stiffness of the substrate. Thus, at $x = 0$, i.e. at the FRP mechanically anchored end, when Eq. (18) is introduced into Eq. (19), the following boundary condition of the debonding problem is obtained regardless its bonded length:

$$\varepsilon_{r0} = \frac{1}{1+r} \cdot \sqrt{2\lambda \cdot G_F \cdot \left(1 - e^{-B \cdot s_0}\right)^2 + C_1} \tag{20}$$

where s_0 is the slip at $x = 0$. Hence, constant C_1 is

$$C_1 = \varepsilon_{r0}^2 \cdot (1+r)^2 - D^2 \cdot \left(1 - e^{-B \cdot s_0}\right)^2. \tag{21}$$

where D is a positive constant given by

$$D = \sqrt{2\lambda \cdot G_F}. \tag{22}$$

Bearing in mind that the FRP composite has a linear constitutive behaviour, introducing Eq. (1) into Eq. (22) yields:

$$C_1 = \varepsilon_{r0}^2 \cdot (1+r)^2 - D^2 \cdot \left(1 - e^{-\frac{B \cdot E_r \cdot A_r \cdot \varepsilon_{r0}}{k}}\right)^2. \tag{23}$$

Therefore, the strains developed in the FRP composite are defined as

$$\varepsilon_r = \frac{1}{1+r} \cdot \sqrt{D^2 \cdot \left(1 - e^{-B \cdot s}\right)^2 + \varepsilon_{r0}^2 \cdot (1+r)^2 - D^2 \cdot \left(1 - e^{-\frac{B \cdot E_r \cdot A_r \cdot \varepsilon_{r0}}{k}}\right)^2}. \tag{24}$$

To define the interfacial slips developed within the interface, Eq. (18) is rewritten as

$$\frac{ds}{\sqrt{(1-e^{-B\cdot s})^2+\left(\frac{\sqrt{|C_1|}}{D}\right)^2}}=D dx, \tag{25}$$

which when integrated leads to

$$\frac{D\cdot \operatorname{arsinh}\left(\frac{\left(D^2+C_1\right)\cdot e^{B\cdot s}-D^2}{\sqrt{|C_1|}\cdot D}\right)}{B\cdot\sqrt{|D^2+C_1|}}=D\cdot x+C_2, \tag{26}$$

where C_2 is another constant to be defined by the interfacial slip developed at the FRP mechanically anchored end, i.e., at point $x = 0$ the interfacial slip is $s = s_0$. Solving Eq. (26) with respect to s, the interfacial slips of the FRP-to-substrate is obtained by

$$s(x)=\frac{1}{B}\cdot\ln\left[\frac{D^2+\sqrt{|C_1|}\cdot D\cdot\sinh\left(\frac{B\cdot(D\cdot x+C_2)\cdot\sqrt{|D^2+C_1|}}{D}\right)}{|D^2+C_1|}\right] \tag{27}$$

where

$$C_2=\frac{D\cdot\operatorname{arsinh}\left(\frac{\left(D^2+C_1\right)\cdot e^{B\cdot s_0}-D^2}{\sqrt{|C_1|}\cdot D}\right)}{B\cdot\sqrt{|D^2+C_1|}}. \tag{28}$$

Introducing Eq. (27) into Eq. (24), the strains developed in the FRP composite are

$$\varepsilon_r(x)=\frac{1}{1+r}\cdot\frac{\sqrt{|C_1+D^2|}\cdot\cosh\left(\frac{B\cdot(D\cdot x+C_2)\cdot\sqrt{|C_1+D^2|}}{D}\right)}{\sinh\left(\frac{B\cdot(D\cdot x+C_2)\cdot\sqrt{|C_1+D^2|}}{D}\right)+\frac{D}{\sqrt{|C_1|}}}. \tag{29}$$

To obtain now the bond stresses developed throughout the bonded joints, Eq. (27) is introduced into Eq. (10) leading to

$$\begin{aligned}\tau_b(x)=2B\cdot G_F\cdot&\frac{\frac{D}{\sqrt{|C_1|}}+\frac{\sqrt{|C_1|}}{D}}{\frac{D}{\sqrt{|C_1|}}+\sinh\left(B\cdot(D\cdot x+C_2)\cdot\sqrt{\left|1+\frac{C_1}{D^2}\right|}\right)}\\&\times\left(1-\frac{\frac{D}{\sqrt{|C_1|}}+\frac{\sqrt{|C_1|}}{D}}{\frac{D}{\sqrt{|C_1|}}+\sinh\left(B\cdot(D\cdot x+C_2)\cdot\sqrt{\left|1+\frac{C_1}{D^2}\right|}\right)}\right)\end{aligned} \tag{30}$$

To obtain the strains developed in the substrate the following expression derived by the authors elsewhere [51,69,70] can be used, i.e.

$$\varepsilon_s=-\frac{1}{1+\frac{1}{r}}\cdot\frac{ds}{dx}. \tag{31}$$

Thus, Eq. (31) can be rewritten as

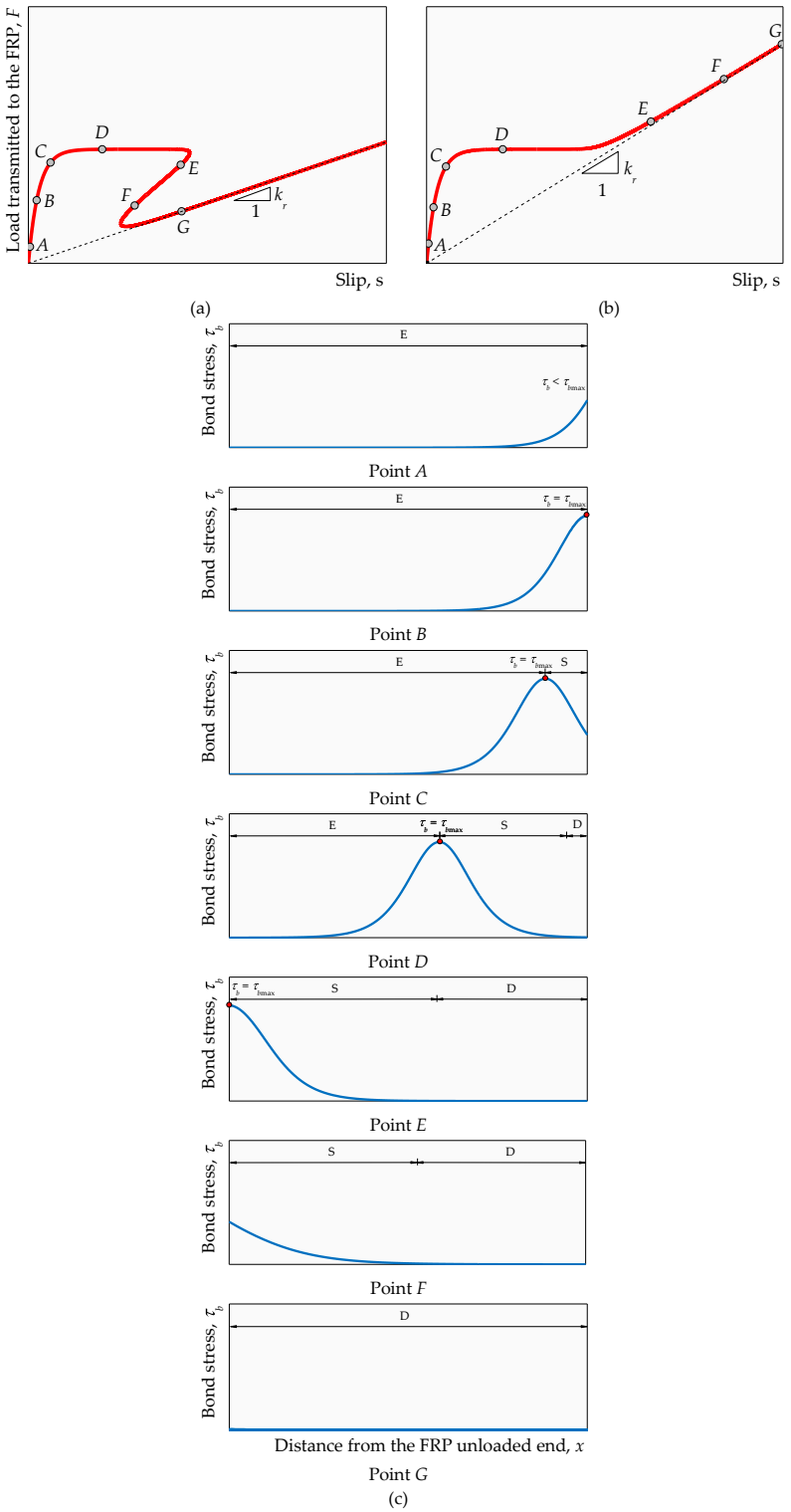

Fig. 5. Debonding process of an FRP-to-substrate with an end anchorage: (a) load-slip curve with low k_r; (b) load-slip curve with high k_r; and (c) bond stress distribution in the debonding process.

$$\varepsilon_s(x) = -\frac{1}{1+\frac{1}{r}} \cdot \frac{\sqrt{|C_1+D^2|} \cdot \cosh\left(\frac{B\cdot(D\cdot x+C_2)\cdot\sqrt{|C_1+D^2|}}{D}\right)}{\sinh\left(\frac{B\cdot(D\cdot x+C_2)\cdot\sqrt{|C_1+D^2|}}{D}\right) + \frac{D}{\sqrt{|C_1|}}}. \tag{32}$$

2.5. Description of the debonding process

The complete debonding process is generically illustrated in Fig. 5. Each state of the debonding process is shown and each one is correlated with the load-slip curve shown in the same figure. At the same time, two distinct scenarios are presented. One where the stiffness of the end anchorage is not sufficiently stiff to prevent the snap-back phenomenon (see Fig. 5a) and the other where the stiffness of the end anchorage is so high that prevents the appearance of the snap-back phenomenon in the load-slip curve of the joint (see Fig. 5b).

Therefore, the debonding process of the end anchored FRP-to-substrate joints begins with a low load transmitted to the FRP composite and with $s < s_{\max}$, the bonded length is fully under an Elastic (E) state (see the first graph in Fig. 5c, Point *A*). Consequently, the bond stresses developed throughout the bonded length are all lower than the maximum bond stress ($\tau_{b\max}$). However, in the regions close to the FRP mechanically anchored end where the bond stresses are quite marginal, the deformations could be ignored and this region could be considered as an undeformed state. In this E state, the load-slip curve is almost linear. As the loads transmitted to the FRP composite increase, the maximum bond stress of the interface is reached at the FRP loaded end (see second graph in Fig. 5c, Point *B*).

Afterwards, the interface enters the Elastic-Softening (E-S) state, which is characterised by an E stage and an S stage that develop at the FRP mechanically anchored end and loaded end, respectively (see third graph in Fig. 5c, Point *C*). In this E-S state, the load-slip curve shows a nonlinear trend with a clear decrease in stiffness.

The debonding of the adherends can be considered when the bond stresses developed in the interface are marginal. Thus, as the maximum bond stress moves towards the FRP mechanically anchored end, the S region increases and the marginal bond stresses closed to the FRP loaded end appear, which means that the interface is under the Elastic-Softening-Debonding (E-S-D) state (see fourth graph in Fig. 5c, Point *D*). Now, the stiffness of the load-slip curve is null, which means that a plateau at the maximum debonded load can be seen. The length of this plateau in the load-slip curve is longer or shorter depending if the bonded length is longer or shorter, respectively. So, if the bonded length is short, i.e. shorter than the effective bond length, no plateau will be seen in the load-slip curve and the debonded load will be lower than the maximum debonded load of the joint.

The bond stress will tend to migrate to the FRP mechanically anchored end and, therefore, the E stage will tend to disappear. When this occurs, the maximum bond stress is located at the FRP mechanically anchored end and the interface is now under the Softening-Debonding (S-D) state (see fifth graph in Fig. 5c, Point *E*). Depending on the stiffness of the end anchorage, the shape of the load-slip curve follows different paths. If the stiffness of the end anchorage is low, then the loads and the slips tend to decrease and the snap-back can be observed (see Fig. 5a). On the other end, if the stiffness of the end anchorage is high, then the loads transmitted to the FRP composite tend to increase with the slips and no snap-back can be observed in the load-slip curve (see Fig. 5b). To define the limit beyond which the snap-back would not increase, constant C_1 should be greater than to or equal to zero, which is the same condition of a rigid end anchorage, i.e., with a slip constraint. Thus, from Eq. (23), the following equality is obtained

$$k \geqslant \frac{B\cdot E_r\cdot A_r\cdot \varepsilon_{r0}}{\ln\left(\frac{D}{D-\varepsilon_{r0}\cdot(1+r)}\right)}. \tag{33}$$

With the exception of ε_{r0} in Eq. (33), all the other parameters are constant. So, the minimum value of k is obtained when ε_{r0} is minimum, i.e., when $\varepsilon_{r0} \to 0$. After applying L'Hopital's rule yields:

$$k_{\min} = B\cdot b_r\cdot\sqrt{\frac{2G_F}{\lambda}}. \tag{34}$$

As the bond stresses continue to migrate towards the FRP unloaded end, the bond stresses developed in the interface are now lower than $\tau_{b\max}$. The complete debonding of the interface can be considered when the bond stresses are too small and can be ignored. Therefore, the interface is under the Debonding (D) state and the load transmitted to the end anchorage is the same as the load transmitted to the FRP composite (see sixth graph in Fig. 5c, Point F). Hence, the slope of the load-slip curve will tend to

$$k_r = \frac{E_r\cdot A_r}{L_b}\cdot\left(s_{L_b} - s_0\right) \tag{35}$$

where L_b is the bonded length; s_{Lb} and s_0 are the interfacial slips at $x = L_b$ and $x = 0$, respectively. It should be noted that since the axial stiffness of the substrate is higher than the axial stiffness of the FRP composite, it would be expected that the failure of the interface can be reached when the end anchorage cannot resist further or when the FRP rupture strain is reached.

3. Validation with the FEM

For the validation of the proposed analytical approach, two bonded lengths (one shorter and another one longer than the effective bond length) and four different end anchorage stiffnesses are considered: $k_0 \to 0$, $0 < k_0 < k_{0\min}$, $k_{0\min} < k_0 < \infty$, and $k_0 \to \infty$. To facilitate the understanding of the debonding process, the materials and their dimensions are fixed. Thus, a CFRP composite and a steel substrate are considered. A commercial package based on the Finite Element Method (FEM) is used so the proposed analytical approach could be validated. Therefore, a brief description of the numerical modelling adopted in this work is reported in this section as well.

Since it is known the deviation of a theoretical result from experimental data is parameter sensitive, the Integral Absolute Error (IAE) is used on the validation of the proposed analytical approach. Nevertheless, it has been used also for model assessment, e.g. [70–72] and IAE values lower than 10 % may indicate that the analytical approach is sufficiently close to the data provided by the FEM. The IAE is calculated according to:

$$IAE = \sum_{s=1}^{n} \frac{\left| d^{PAA} - d^{FEM} \right|}{\sum_{s=1}^{n} d^{FEM}} \tag{36}$$

where d^{PAA} and d^{FEM} correspond to the data obtained from the proposed analytical approach and those calculated from the FEM, respectively; and n corresponds to the number of measurements carried out during the simulations of the debonding process.

3.1. Mechanical properties of the materials and dimensions of the specimens

In this study, an unidirectional CFRP composite used by the authors in another work [73] is herein considered. The mechanical properties in the direction of the fibres are as follows: elastic modulus of 159 GPa, tensile strength of 1,565 MPa, and a rupture strain approximately equal to 1.0 %. The strip of the CFRP composite has a thickness of 1.4 mm and a width of 10 mm and it was bought from a local S&P supplier.

For the substrate, a hollowed rectangular steel profile with an elastic modulus of 200 GPa and yielding strain of 0.2 % is considered. The steel profile has 150 mm of side and with a thickness of 7 mm. The axial stiffness ratio of the studied specimens is $r = 0.01$. To bond the CFRP strip to the steel profile, an epoxy resin S&P220 is considered which, according to another work of the authors [73], leads to a local adherence that can be approximated by an exponential bond-slip relationship. As already mentioned before, this bond-slip relationship was originally proposed by Dai et al. [12] and to define it the following parameters were used: $B = 17.33$ mm^{-1}, mode II fracture energy of $G_F = 1.783$ N/mm, maximum bond stress of 15.45 MPa.

For the definition of the bonded length of the CFRP-to-steel joints, the effective bond length was taken into account. Thus, from a previous work of the authors [48], the effective bond length of the CFRP-to-steel joints in which an epoxy resin S&P220 with 1.4 mm of thickness is used, is approximately 157 mm. Thus, two bonded lengths of 50 mm and 250 mm are assumed, which represent, respectively, two cases with shorter and longer bonded lengths, i.e., shorter and longer than the effective bond length of the CFRP-to-steel joints.

3.2. Identification of the specimens

To facilitate the readership of the text, each specimen is identified by a particular nomenclature that identifies the materials, stiffness of the end anchorage and the axial stiffness ratio of the materials. For instance, specimen CS250-r0.01-*k*10,000 intends to identify the specimen where a CFRP strip is externally bonded to a steel substrate (CS) in which the axial stiffness between the CFRP strip and the steel substrate is $r = 0.01$ and the stiffness of the end anchorage is $k = 10{,}000$ N/mm. Table 1 summarizes the ID of the specimens used in this work.

Table 1
ID of the specimens.

ID	Bonded length, L_b (mm)	Stiffness of the end anchorage, k_0 (N/mm)
CS50-r0.01-k0	50	0
CS50-r0.01-k10,000		10,000
CS50-r0.01-k100,000		100,000
CS50-r0.01-k200,000		200,000
CS50-r0.01-k∞		∞
CS250-r0.01-k0	250	0
CS250-r0.01-k10,000		10,000
CS250-r0.01-k100,000		100,000
CS250-r0.01-k200,000		200,000
CS250-r0.01-k∞		∞

3.3. Numerical modelling with the Finite Element Method

To model the debonding process of CFRP-to-substrate different commercial software have been used successfully in the literature, e.g. [8,9,74–78]. Since it has proven its ability to estimate the bond behaviour between two adherends subjected either to pull-pull or pull–push tests, e.g. [34,35,69,79], the Finite Element commercial software ATENA package [80] was used in this work. This software has a 2D and a 3D version and the 2D version was chosen so the number of unknowns and nonlinear equations to be solved by the Newton-Raphson method could be reduced significantly. Moreover, the 2D version is the most approximated version of the proposed analytical approach, which makes it closer to the initial assumptions of the proposed analytical approach. Additionally, the number of finite elements of the model is reduced significantly, which reduces the calculation time taken for processing a single model with no loss of precision in the simulations [69,79].

To simulate the contact between two materials, ATENA software [80] uses a coupled cohesive model based on the Mohr-Coulomb rupture criterion with tension cut-off. This means that, in the presence of peeling stresses (in the direction coincident with mode I), the bond stresses associated with mode II follow the Mohr-Coulomb criterion. The friction angle (ϕ) of the interface is another parameter that needs to be defined since it significantly influences the bond performance of the joints when subjected to a mixed mode situation, i.e., mode I + II [34,35].

To simulate the loads applied to the CFRP strip, a regular monotonic displacement of 0.002 mm per step was considered and applied to the right hand of the CFRP end as can be seen in Fig. 6. To control the simulations, three monitoring points were considered. The first one is placed at the same point of the displacement control and the second and third monitoring points control the loads transmitted to the CFRP composite and to the spring, respectively. To control the loads transmitted to the CFRP composite the monitoring point was placed at the midpoint of the reaction steel plate (see 2 in Fig. 6). The complete debonding of each simulated specimen was reached regardless of the number of steps considered in each simulation.

Near the contact between adherends, the models in ATENA software [80] were discretized with meshes with 0.4–0.5 mm quadrilateral finite elements (with smooth element shapes). Since the specimens have different bonded lengths, the number of finite elements used in each model was different. So, the number of finite elements in the models with $L_b = 50$ mm had the fewest (i.e., 2613) finite elements, whereas the models with $L_b = 350$ mm had the highest number (i.e., 12613) of finite elements. In an Intel Core i7-7700HQ laptop computer at 2.80 GHz with 16 GB of 2400 MHz RAM, the simulations were carried out for a minimum of approximately 20 min (in the specimens with the lowest number of finite elements) to 60 min (in the specimens with the highest number of finite elements).

3.4. Load-slip curves

The load-slip curves of the CFRP-to-steel bonded joints with the shortest and longest bonded lengths are shown in Fig. 7, i.e., with $L_b = 50$ mm and $L_b = 250$ mm. The load-slip curves allow us to observe also the influence of the stiffness of the spring on the CFRP-to-steel bonded joints. In the case of the specimens with the shortest bonded lengths no snap-back regardless of the stiffness of the spring can be seen. However, in the case of the specimens with the longest bonded lengths it can be seen that as the stiffness of the spring increases, the snap-through and snap-back phenomena tend both to disappear. Thus, in these specimens, after the debonding of the CFRP from the steel substrate begins, the plateaux seen in Fig. 7b, the loads tend to increase once again with the slips. This load increase is linear with the slips, which has a slope determined by Eq. (35) and it means that no bond stresses are being transferred between the CFRP composite and the steel substrate.

Considering that the stiffness of the steel substrate is too high when compared with the CFRP composite, the yielding of the steel is not expected. Therefore, three main failure modes can be identified by the proposed analytical approach: (i) cohesive debonding of the interface; (ii) spring rupture; and (iii) CFRP rupture. Unless the stiffness of the spring is quite high (or infinite), the first two possible failure modes are more likely to occur. Still, two different paths can be identified here. The first one corresponds to the case where the interface completely debonds from the substrate and the maximum load transmitted to the CFRP composite (F_{max}) does not exceed the debonding load (F_{db}) due to the failure of the spring. The other is the case that, after complete debonding of the CFRP composite from

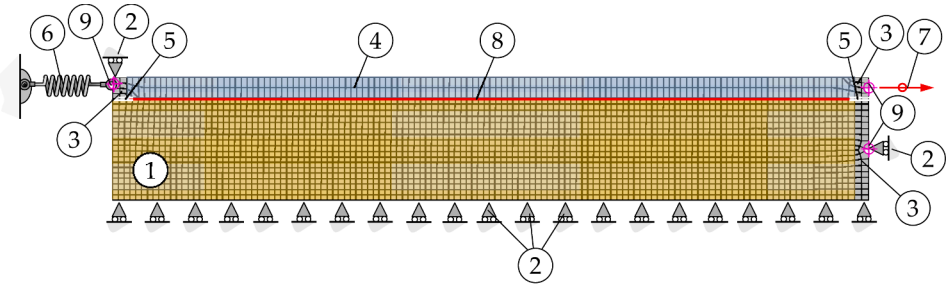

Key: 1 – Steel substrate; 2 – Roller support; 3 – Rigid material; 4 – CFRP composite; 5 – Interface with no contact; 6 – End anchorage (spring); 7 – Displacement control; 8 – Interface element; 9 – Load/reaction monitoring point.

Fig. 6. Example of the finite element mesh of the CFRP-to-steel specimens CS50-W10-r0.01-k0|10,000|100,000|200,000|∞.

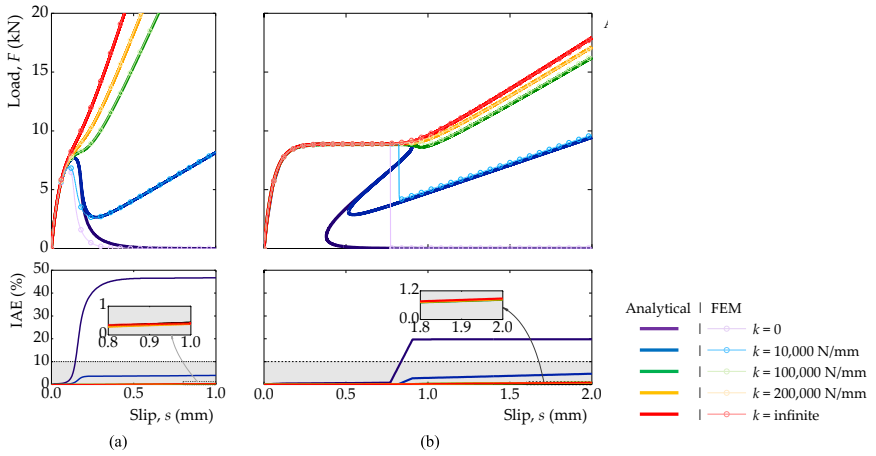

Fig. 7. Accuracy of the load-slip curves obtained by the proposed analytical approach with the FEM when: (a) $L_b = 50$ mm; and (b) $L_b = 250$ mm.

the substrate, the maximum load transmitted to the CFRP composite exceeds the debonding load. So, it can be defined by an effective stiffness (k_{eff}), i.e., the stiffness of the spring beyond which the maximum load transmitted to the FRP composite is higher than the debonding load. Thus, based on Eq. (34), $k_{\min} = k_{eff} = 133{,}631$ N/mm.

The IAE values barely exceeded 10 %, which shows the high accuracy of the analytical approach with the FEM. Nevertheless, The two situations where the IAE is higher than 10 % correspond to the case of $k \to 0$. In the case of $L_b = 50$ mm (i.e., CS50-r0.01-k0), the post-peak behaviour obtained by the analytical approach overestimates the results obtained by the FEM, which explains the higher IAE values. However, in the case of $L_b = 250$ mm (i.e., CS250-r0.01-k0), the higher IAE values are mainly due to the snap-back phenomena. Once the load decay to zero in the FEM, the analytical approach estimates, despite not meaningfully, a longer plateau at the maximum load and the difference between both methods in that slip interval is huge and explains the abrupt increase of the IAE value observed there.

4. Comparison with other studies

To check the wide applicability of the proposed analytical approach, five different studies available in the literature were considered [27,29,37,38,42]. In these studies, experimental, numerical and analytical data describing the bond behaviour of mechanically anchored FRP-to-substrate are considered. Thus, mechanically anchored CFRP-to-concrete [27,29,38], CFRP-to-steel [42], and CFRP-to-timber [37] bonded joints are analyzed thoroughly.

4.1. *Tests carried out by Lu et al. [38]*

The experimental tests and analytical as well as numerical simulations carried out by Lu et al. [38] are modelled here with the proposed analytical approach. Lu et al. [38] have reported the test of CFRP-to-concrete joints anchored with a CFRP U-wrap jacket. The

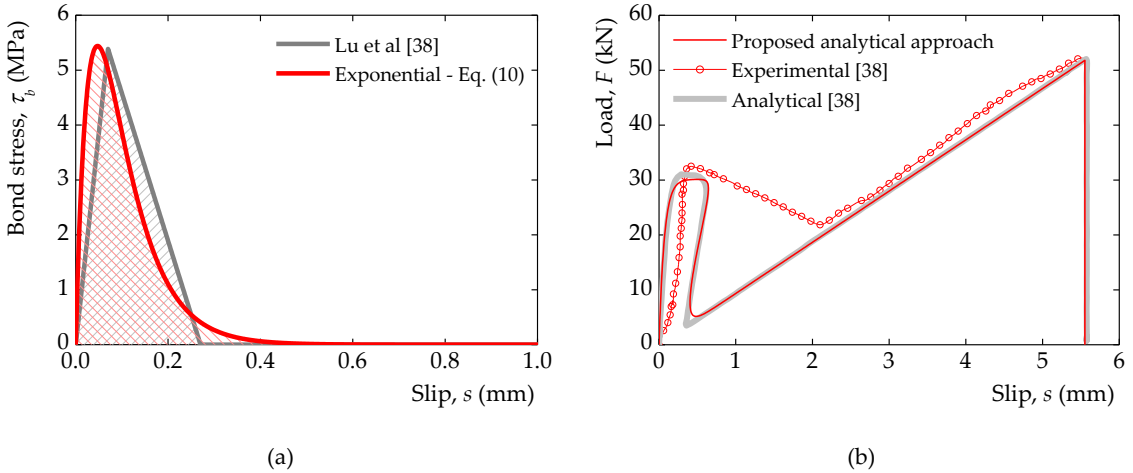

Fig. 8. Comparison with the work carried out by Lu et al. [38]: (a) bond-slip relationships; and (b) load-slip curves.

single-lap shear tests consisted of a CFRP composite with a cross-sectional area of 1.2×50 mm^2 (thickness × width) externally bonded to a concrete block with a $300 \times 220 \times 700$ mm^3 (thickness × width × length) throughout a bonded length of 300 mm. Only the elastic moduli of the adherends are reported, i.e. 205 GPa and 33 GPa for the CFRP composite and concrete, respectively. Although the authors [38] have not reported the bond-slip relationship obtained experimentally, they assumed a classical bond-slip relationship with a triangular shape. Thus, the maximum bond stress is 5.44 MPa with a maximum and ultimate slip of 0.071 mm and 0.273 mm, respectively, which corresponds to a fracture energy of 0.743 N/mm. The authors [38] also reported a stiffness of the end anchorage of 12,100 N/mm with an ultimate slip of 4.30 mm.

Thus, to make feasible comparisons with the work carried out by Lu et al. [38], the exponential bond-slip relationship defined in Eq. (10) was adjusted, through a minimization process where the fracture energy was used as a constraint, to the triangular bond-slip relationship of the authors [38] leading to $B = 14.64$ mm^{-1}, $\varepsilon_{r\max} = 0.245$ %, and $s_{\max} = 0.047$ mm. Both bond-slip relationships are shown in Fig. 8a.

The load-slip curve obtained by the proposed analytical approach is compared with the analytical model and experimental data reported by Lu et al. [38] (see Fig. 8b). As can be seen, both analytical approaches provided quite close results and both are consistent with the experiment. Nevertheless, it should be mentioned that since the analytical approach developed by Lu et al. [38] is based on a triangular bond-slip relationship, it requires the derivation of a large number of equations so each state that the mechanically anchored bonded joint will undergo until its failure could be defined. Therefore, the proposed analytical model is much easier to use and implement due to the single function (exponential) used to describe the local bond behaviour of the joints.

Lu et al. [38] have also reported the axial and bond stress and distributions for four particular loads of the debonding process: 10.54 kN, 21.84 kN, 29.04 kN, and 35.90 kN. The comparison between the proposed analytical approach and the results reported by Lu et al. [38] is shown in Fig. 9. The results provided by the proposed analytical approach also show a good agreement with those reported by Lu et al. [38]. As seen from Fig. 9a, with the proposed analytical approach the axial stresses are in fair agreement with the experimental data. For the two first lower loads transmitted to the CFRP composite, the axial stresses mainly develop at the CFRP-loaded end. However, for $F = 29.01$ kN a plateau at maximum axial stress can be observed. This means that the debonding of the interface has begun. When $F = 35.90$ kN is transmitted to the CFRP composite, the CFRP-to-concrete joints are completely debonded and the load transmitted to the spring (U-wrap jacket) equals the load transmitted to the CFRP composite.

From Fig. 9b it can be seen that the bond stresses developed throughout the bonded length has always a continuous derivative whereas for the analytical approach proposed by Lu et al. [38] it is possible to identify two points where such a thing does not occur. Thus, looking, at the curve corresponding to $F = 29.01$ kN, it is possible to see the three stages defined by the triangular bond-slip relationship and identify the transition between the E stage to the S stage, i.e. where the maximum bond stress occurs, and the transition between the S stage to the D stage, i.e. where the bond stresses become zero. Therefore, to capture this E-S-D state of the bonded joint, it is needed to analytically define the E, S and D stages, whilst it takes only one formula to define this E-S-D or any other state of the interface with the proposed analytical approach (see Eq. (30)).

Lu et al, [38] have also carried out a parametric study where the authors checked the effects of the bonded length, stiffness of the end anchorage, and stiffness of the FRP composite. The proposed analytical approach was used to replicate each case studied by Lu et al. [38]. Thus, regarding the effect of the stiffness of the end anchorage, Fig. 10a compares the results obtained by both approaches. Four different cases with different stiffnesses of the end anchorage were simulated: 0 N/mm, 6,500 N/mm, 12,100 N/mm, and 18,150 N/mm. The results show good agreement and it can be seen also that the ultimate load (F_{tl}) increased with the stiffness of the end anchorage. However, two different cases can be identified. One where the ultimate load of the joint correspond to the debonded load

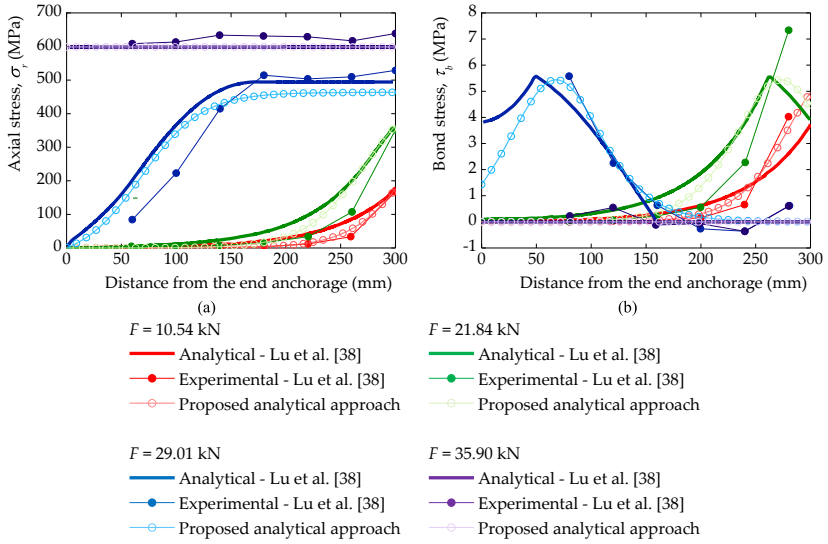

Fig. 9. Comparison with the bond stresses developed throughout the bonded length.

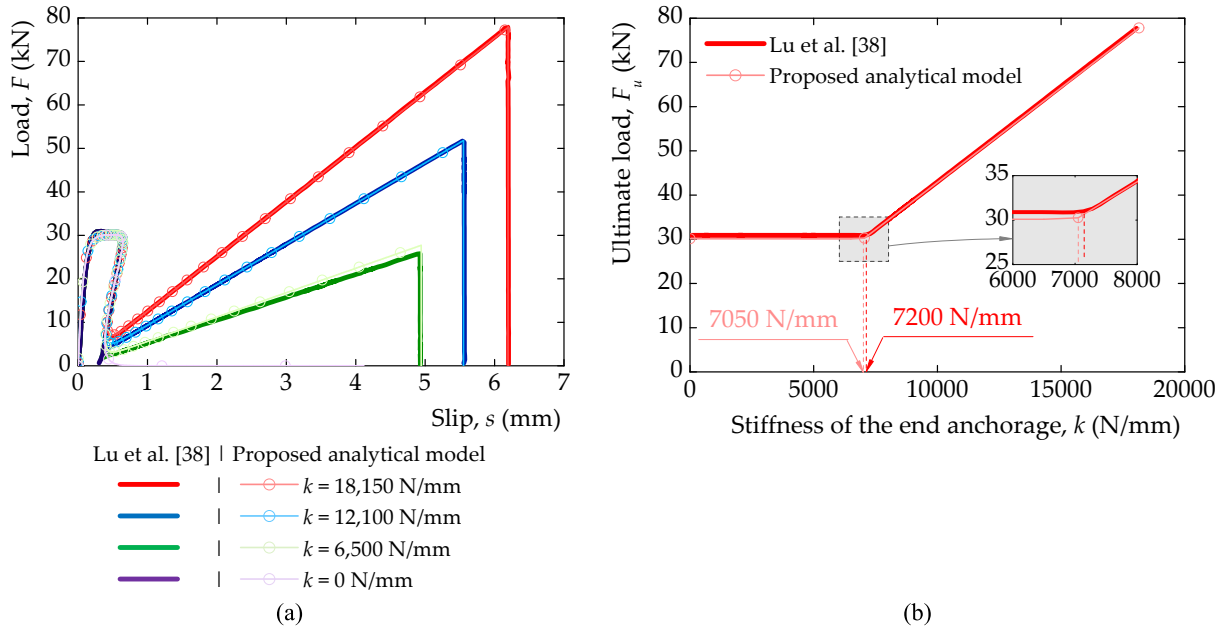

Fig. 10. Effect of the stiffness of the end anchorage (k): (a) comparison with the load-slip curves; and (b) comparison with the ultimate load.

(F_{db}), i.e., to the maximum load needed to debond the FRP composite from the substrate. In this case, at the instant of the spring failure, the load is lower than the debonded load and, therefore, the end anchorage is useless since it is not able to increase the strength of the joint. The other corresponds to the case where the ultimate load is higher than the debonded load and the ultimate load was increased due to the influence of the end anchorage, improving, therefore, the bond performance of the mechanically anchored bonded joint. Thus, to calculate the minimum stiffness of the end anchorage the debonded load should be equal to the ultimate load given by Eq. (1). Therefore, considering that the debonded load can be given by [81]:

$$F_{db} = \begin{cases} b_r \cdot \sqrt{2G_F \cdot E_r \cdot t_r \cdot (1+r)} & \text{if} \quad L_b \geqslant L_{eff} \\ \beta_L \cdot b_r \cdot \sqrt{2G_F \cdot E_r \cdot t_r \cdot (1+r)} & \text{if} \quad L_b < L_{eff} \end{cases} \tag{37}$$

where, according to some authors, e.g. [81–83], β_L can be obtained according to

$$\beta_L = \frac{L_b}{L_{eff}} \cdot \left(2 - \frac{L_b}{L_{eff}}\right), \tag{38}$$

$$\beta_L = \sin \cdot \left(\frac{\pi}{2} \cdot \frac{L_b}{L_{eff}}\right), \tag{39}$$

or

$$\beta_L = \frac{\arctan\left(2\pi \cdot \frac{L_b}{L_{eff}}\right)}{\arctan(2\pi)}, \tag{40}$$

where L_{eff} is the effective bond length of the joint.

Therefore, equating Eq. (37) to Eq. (1), the effective stiffness of the end anchorage (k_{eff}), i.e., the stiffness beyond which the end anchorage actually can improve the load transmitted to the FRP composite is

$$k_{eff} = \begin{cases} \dfrac{b_r \cdot \sqrt{2G_F \cdot E_r \cdot t_r \cdot (1+r)}}{s_0} & \text{if} \quad L_b \geqslant L_{eff} \\ \dfrac{\beta_L \cdot b_r \cdot \sqrt{2G_F \cdot E_r \cdot t_r \cdot (1+r)}}{s_0} & \text{if} \quad L_b < L_{eff} \end{cases} \tag{41}$$

where $s_0 = s_u$, i.e., the ultimate slip that can occur in the spring (or end anchorage).

Fig. 10b identifies the k_{eff} of the mechanically anchored CFRP-to-concrete bonded joints. From Eq. (41), a value of 7050 N/mm was calculated which is less than 2.1 % of the value determined by Lu et al. [38]. Moreover, for values higher than k_{eff}, the increase of the

ultimate load has a linear trend, which the proposed analytical approach was also able to capture and confirm the results achieved by Lu et al. [38].

The effect of the bonded length was also shown previously in Subsection 3.4. However, Fig. 11 shows that the increase in the bonded length does not increase the ultimate load. Moreover, Fig. 11 shows that the results obtained by the proposed analytical model are in agreement with those obtained by Lu et al. [38] and all the adopted bonded lengths are longer than the effective bond length since the debonded load was reached in the four different bonded lengths of 200 mm, 300 mm, 400 mm, and 500 mm.

Fig. 12 shows the effect of the reinforcement stiffness ($E_r t_r$) on the bond behaviour of four different cases: 12,300 N/mm, 24,600 N/mm, 49,200 N/mm, and 73,800 N/mm, i.e. with $r = 0.003$, 0.006, 0.011, and 0.017, respectively. The bonded length of 300 mm was fixed. The results obtained from the proposed analytical approach continue aligned with those obtained by Lu et al. [38]. It can be seen also that the increase of the FRP stiffness increases the debonded load. The plateau observed, e.g., in the specimen with an FRP stiffness of 12,300 N/mm was reduced with the increase of the FRP stiffness. This can be explained by the increase of the effective bond length of the joint, which increases with the FRP stiffness [15,39,81,84–88]. In these studied cases, the increase of the FRP stiffness was not sufficient enough to change the ultimate load of the joints. However, these results show that as the stiffness of the reinforcement increases, more crucial will be to adopt a stiffer end anchorage so the final strength of the mechanically anchored bonded joint can be effectively increased.

4.2. *Tests carried out by Mazzotti et al. [29]*

Mazzotti et al. [29] carried out a series of tests with CFRP-to-concrete mechanically anchored joints. The authors [29] studied the influence of the concrete surface preparation and used a steel plate as an end anchorage. The concrete block has 150 × 200 × 600 mm^3 (width × thickness × length) and a mean elastic modulus of 30.7 GPa, mean tensile strength of 3.81 MPa and compressive strength of 52.7 MPa. The CFRP strip with a cross-sectional area of 1.2 × 80 mm (thickness × width) was externally bonded to the concrete block. Only the CFRP mean elastic modulus of 195.7 GP was reported by the authors [29]. To model the bond between the CFRP and the concrete block, Mazzotti et al. [29] used the Popovics' formula [89], which was originally used to model the stress–strain relationship of concrete under tension. Therefore, the exponential bond-slip relationship in Eq. (10) was approximated to the original bond-slip relationship, through a minimization process where the fracture energy of 0.39 N/mm determined from the tests is used as a constraint. Thus, the following parameters were obtained: $B = 32.974$ mm^{-1}, $\tau_{b\max} = 6.43$ MPa, and $s_{\max} = 0.021$ mm.

Fig. 13 compares the load-slip curves obtained by Mazzotti et al. [29] with those obtained by the proposed analytical approach. It should be noted that beyond the experimental data, Mazzotti et al. [29] numerically simulated their experiments assuming a rigid end anchorage. However, after the joints' debonded load (Fdb), the subsequent load increase in the numerical simulations has a higher slope than that obtained experimentally. This may indicate that the end anchorage could not be considered rigid, which could be attributed, e.g., to the short length of the steel anchorage or the low external pressure applied to the anchorage. However, neither the grip length nor the external pressure applied to the anchorage was reported by the authors]29]. For this reason, an alternative and more realistic elastic stiffness for the end anchorage was investigated. Hence, to obtain the same slope after the debonding of the CFRP composite from the concrete block, a stiffness of approximately 225,000 N/mm for the end anchorage was obtained by a trial and error process. The rigid end anchorage was also simulated.

The results obtained by the proposed analytical approach are in good agreement with the numerical results obtained by Mazzotti et al. [29]. When assuming the elastic stiffness of the end anchorage of 225,000 N/mm, the results show a snap-back after the debonded load has been reached. Then, the loads increase linearly with the interfacial slips and parallel to the experimental data. Therefore, and as already mentioned, this indicates that the end anchorage used by Mazzotti et al. [29] was not sufficiently rigid to constrain the interfacial slips under the steel plate anchorage.

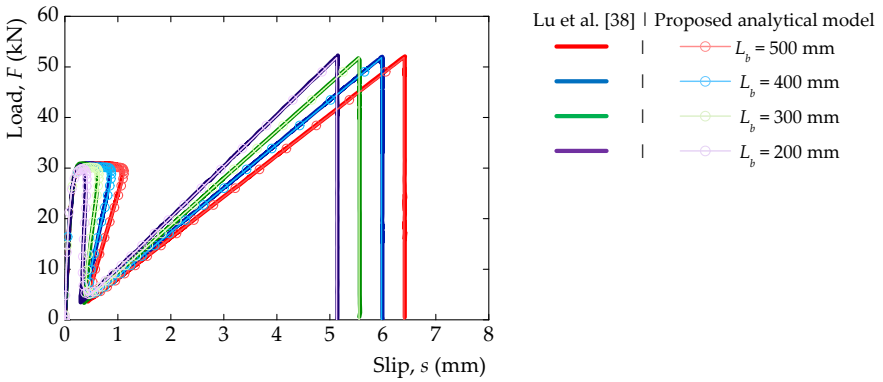

Fig. 11. Effect of the bonded length of the mechanically anchored bonded joints with different bonded lengths of 200 mm, 300 mm, 400 mm, and 500 mm.

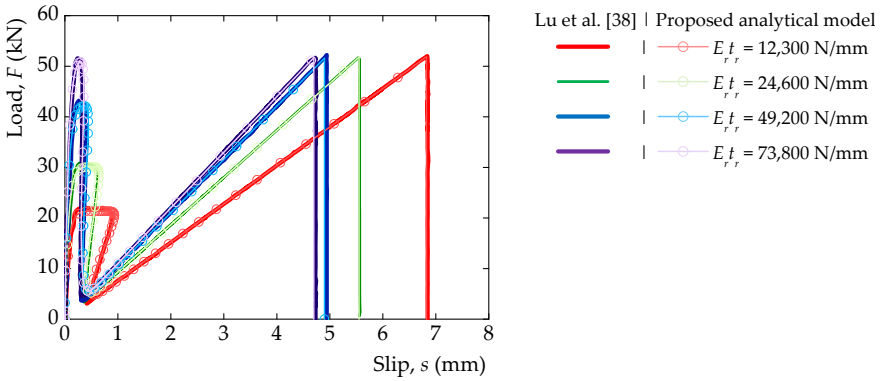

Fig. 12. Effect of the reinforcement stiffness ($E_r t_r$).

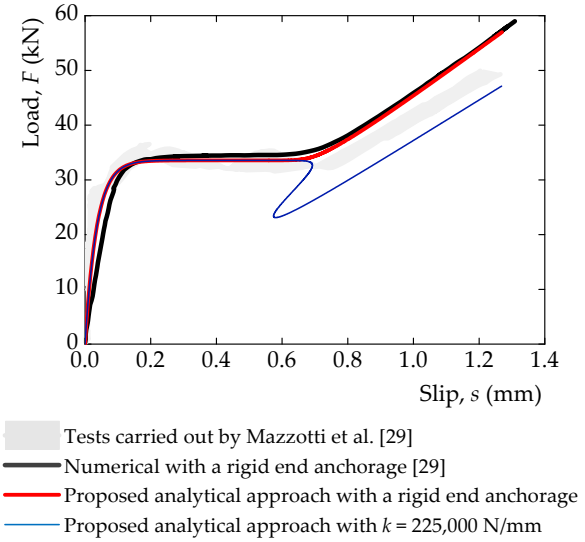

Fig. 13. Comparison between the load-slip curves obtained by Mazzotti et al. [29] and the load-slip curve predicted by the proposed analytical approach.

4.3. Tests carried out by Barris et al. [27]

To understand the bond behaviour of mechanically anchored CFRP-to-concrete joints, Barris et al. [27] conducted an experimental study with a commercial mechanical anchorage and analyzed the influence of the external compression stresses applied to the anchorage. Three CFRP laminates with three different widths were used: 50 mm, 80 mm, and 100 mm. The elastic modulus and the CFRP rupture strain of each composite are summarized in Table 2. A concrete block with 200 × 500 × 800 mm^3 (thickness × width × length) was used as substrate. The mechanical properties of the concrete reported by Barris et al. [27] are as follows: elastic modulus of 24.7 GPa and mean compressive strength of 33.3 MPa.

The experimental load-slip curves of the specimens obtained by Barris et al. [27] are shown in Fig. 14. In all cases, the rupture of the CFRP laminate was predicted by the proposed analytical approach, which confirms the observations made by Barris et al. [27]. After the complete debonding of the CFRP from the concrete block, the experimental data showed a linear trend with a slope equal to the

Table 2
Definition of mechanical properties of the CFRP laminates and the parameters obtained for the definition of the exponential bond-slip relationship of the mechanically anchored CFRP-to-concrete carried out by Barris et al. [27] (average values).

Width of the CFRP, b_r (mm)	Elastic modulus, E_r (MPa)	Rupture strain, ε_r (%)	B (mm^{-1})	Maximum bond stress, τ_{max} (MPa)	Maximum slip, s_{max} (mm)	Fracture energy, G_F (N/mm)
50	176.4	1.25	14.783	4.79	0.047	0.650
80	170.5	1.46	11.690	4.15	0.059	0.710
100	169.4	1.46	12.172	3.53	0.057	0.580

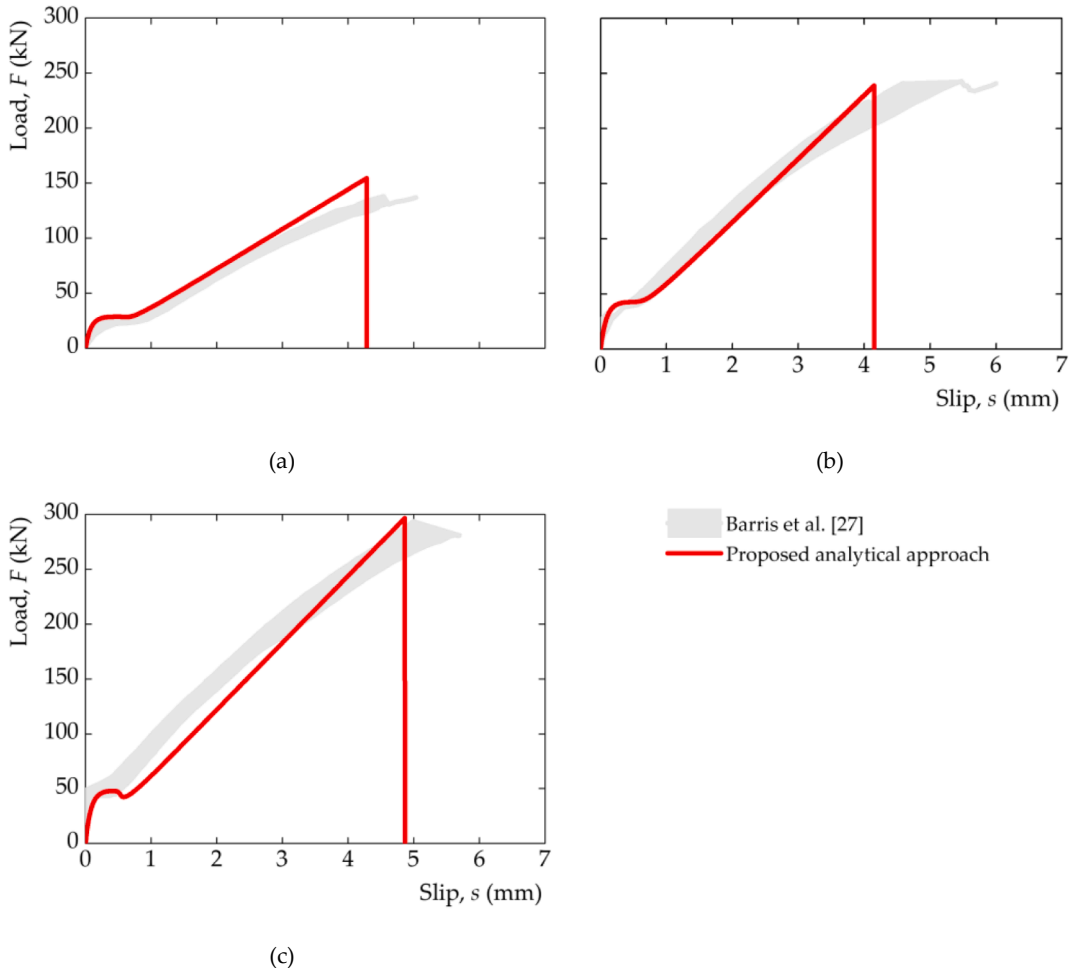

Fig. 14. Comparisons with the load-slip curves obtained by Barris et al. [27]: (a) load-slip curves with a CFRP composite 50 mm wide; (b) load-slip curves with a CFRP composite 80 mm wide; and (c) load-slip curves with a CFRP composite with 100 mm wide; and (d) CFRP strain distributions in specimen L50-T30.

axial stiffness of the CFRP composite. However, as the loads transmitted to the CFRP laminate increased, Barris et al. [27] reported that slips under the mechanical steel plate occurred and a nonlinear stiffness of the load-slip curve was seen until the CFRP rupture.

The bond-slip relationship of the CFRP-to-concrete joints was approximated through the Popovics' formula [89] and, therefore, the exponential bond-slip relationship in (10) was adjusted, through a minimization process where the experimental fracture energy of the

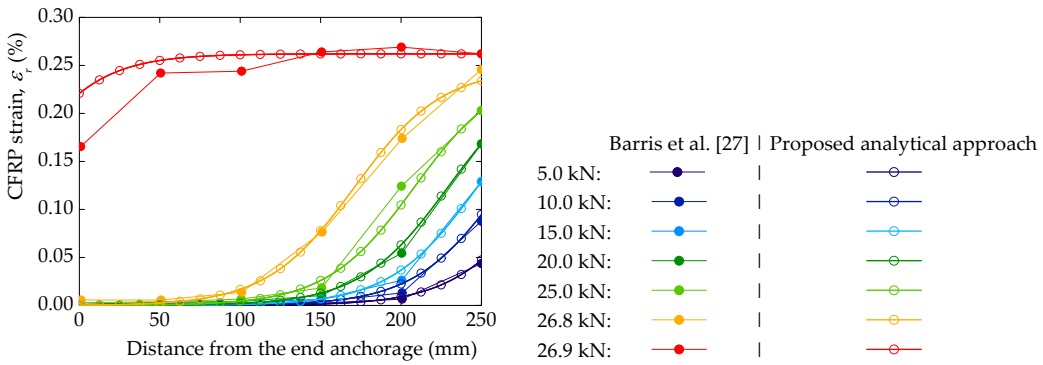

Fig. 15. Comparison between the results obtained from the proposed analytical approach with the experimental data of the CFRP strain distributions in specimen L50-T30 [27].

test was used as a constraint. The parameters needed to define Eq. (10) are summarized in Table 2. The stiffness of the spring was obtained so the initial slope of the load-slip curve could be parallel to the slope obtained from the experiments. Thus, in the mechanically anchored CFRP-to-concrete joints with the CFRP composite 50 mm and 100 mm wide, the stiffness of the end anchorage is approximately 250,000 N/mm, whereas in the other case with $b_r = 80$ mm a stiffness approximately of 500,000 N/mm was obtained. When compared with the experiments, the results obtained by the proposed analytical approach showed a fair agreement with the experimental data as well. However, the spring with a linear behaviour could not fully represent the complete behaviour of the joints after the debonded load. This suggests that a spring with a nonlinear behaviour should be considered rather than an elastic and linear one. It should be noted here that despite this being a topic out of the scope of this work, the proposed analytical can accommodate such spring once the strain-slip relationship of the end anchorage is known. To that end, the nonlinear strain-slip relationship should be considered in the definition of constant C_1 defined in Eq. (21). The subsequent equations depend on this constant, but once determined C_1, all those equations remain valid.

Fig. 15 shows the CFRP strain distributions of the mechanically anchored CFRP-to-concrete joint of specimen L50-T30 [27] for different loads transmitted to the CFRP composite. The analytical results are aligned with the experiments. As expected, the CFRP strains are higher at the CFRP pulled end. Unlike the bonded joints free of any end anchorage where the strains are always zero at the CFRP-free end, here the CFRP strains tend to increase at that same point due to the influence of the anchorage. This can be seen clearly in Fig. 15 when $F = 26.9$ kN. Moreover, since near the CFRP pulled end the CFRP strains are constant, the bond stresses should be zero which means that the CFRP composite has already started to debond from the concrete block.

4.4. Tests carried out by Silva [42]

Silva [42] tested two CFRP-to-steel joints mechanically anchored with a steel plate. In one of the tests, a bonded length of 50 mm was used, whereas a bonded length of 200 mm was used in the second test. However, only in the second case was possible to acquire feasible experimental data due to an anomaly of the data logger during the test of the specimen with the shortest bonded length. The CFRP strip had a cross-sectional area of 1.4×10 mm^2 (thickness $\times$ width) and it was externally bonded to a rectangular hollowed steel profile with 150 mm of side and a thickness of 7 mm. From the uniaxial tension test of four CFRP flat coupons, the mean mechanical properties of the CFRP composite are as follows: elastic modulus of 159 GPa, rupture strain of 1.03 % and tensile strength of 1,565 MPa. The steel was not tested but common values were considered, i.e., an elastic modulus of 200 GPa and yielding strain of 0.2 %. The bond–slip relationship was approximated by Silva [42] to the exponential bond-slip relationship defined in Eq. (10) leading to the following parameters: $B = 13.840$ mm^{-1}, $\tau_{b\max} = 8.52$ MPa, $s_{\max} = 0.050$ mm, and $G_F = 1.231$ N/mm.

The aim of Silva [42] was to obtain a rigid end anchorage and the mechanical steel plate was attached against the CFRP-to-steel joint. However, the external pressure applied to the steel plate was not measured but the rupture of a few CFRP fibres was observed during the pressure of the steel plate [42]. The results were also analytically modelled by Silva [42] who derived a particular solution of the proposed analytical approach, i.e., Silva [42] assumed that no slips occur at the CFRP mechanically anchored end. For this reason, a rigid stiffness of the end anchorage was assumed in the proposed analytical approach to simulate the load-slip curve. The results are compared in Fig. 16 and they show a fair agreement with the experimental data.

4.5. Tests carried out by Biscaia and Diogo [37]

In another work of the first author [37], a series of CFRP-to-timber joints with and without a mechanical end anchorage were tested. Different anchorage systems were considered among which the four most efficient were selected to simulate with the proposed analytical approach. Thus, the four selected mechanical anchorages consisted of using: (i) a steel plate; (ii) two superposed L-shaped steel profiles; (iii) an embedded rectangular hollowed metallic profile; and (iv) a CFRP embedded end into the timber core. In each series, three tests were performed under the same test conditions. The CFRP strip used in the tests with the CFRP embedded into the timber core had a thickness of 1.4 mm, whereas, in the other three cases, a CFRP strip with 2.8 mm of thickness was used. Nevertheless, the same CFRP width of 10 mm was used in all specimens. The mean elastic modulus of the CFRP with 1.4 mm of thickness is 169.3 GPa, whereas the thicker CFRP has a mean elastic modulus of 159.6 GPa. The timber prisms have a cross-sectional area of 100×70 mm^2 (thickness $\times$ width) and a height of 500 mm. The mean tensile elastic modulus of the timber is 12.93 GPa.

The experimental bond-slip relationships obtained in each group series previously mentioned were approximated to the exponential bond-slip relationship defined in Eq. (10) through a minimization process where the fracture energy obtained experimentally was fixed. Table 3 summarizes the parameters of the exponential bond-slip relationships obtained for each type of mechanically anchored CFRP-to-timber joints tested by Biscaia and Diogo [37].

Fig. 17 compares the load-slip curves obtained by the proposed analytical approach with the load-slip curves obtained experimentally. To obtain these results, the stiffness of the end anchorage was assumed infinite. Since after the CFRP has debonded from the timber substrate, the load-slip curves tend to be the axial stiffness of the CFRP strip. Thus, these results show that all end anchorages were able to constrain the slips at the CFRP mechanically anchored end. However, the use of two superposed L-shaped steel profiles was able to better approximate the loads transmitted to the CFRP composite to its failure load, whilst the CFRP embedded into the timber core led to the highest interfacial slips of the joints.

5. Conclusions

The present work aims to propose an innovative analytical approach that can predict the bond performance of wide-ranging FRP-

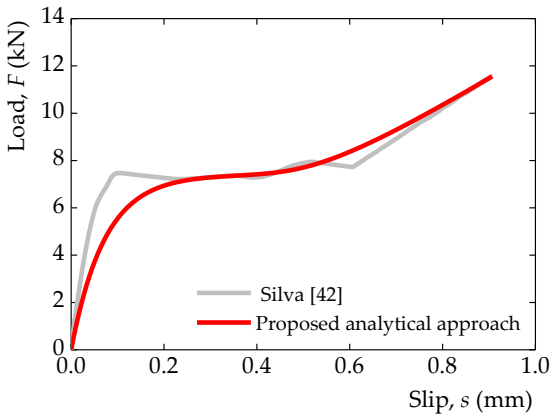

Fig. 16. Comparison between the experimental load-slip curve obtained by Silva [42] and the load-slip curve predicted by the proposed analytical approach.

Table 3
Parameters needed to define the exponential bond-slip relationship of the CFRP-to-timber joints with an end anchorage tested by Biscaia and Diogo [37].

Mechanical anchorage type	Thickness of the CFRP, t_r (mm)	B (mm^{-1})	Maximum bond stress, τ_{max} (MPa)	Maximum slip, s_{max} (mm)	Fracture energy, G_F (N/mm)
Steel plate	2.8	7.576	15.04	0.092	3.970
Embedded rectangular hollowed metallic profile	2.8	9.000	14.25	0.077	3.166
Two superposed L-shaped steel profiles	2.8	8.339	12.71	0.083	3.048
CFRP embedded end	1.4	4.750	9.69	0.146	4.080

to-substrate joints, including with and without an end anchorage with a linear behaviour. To that end, a series of closed-form solutions to predict the load-slip curves, slip, FRP or substrate strains and bond stress distributions are proposed. To validate the proposed analytical approach, the FEM was used as well as the analytical, numerical and experimental data available in the literature. Hence, several types of mechanically anchored joints with no end anchorages were considered in the validation of the proposed analytical approach. Based on the results achieved in this work, the following main conclusions can be drawn:

- The simplicity and wide-ranging application of the proposed analytical approach as well as its good agreement with the results provided by the FEM, and other analytical, numerical and experimental results were shown;
- The full debonding process of an FRP-to-substrate with and without an end anchorage can be described with a single expression which no other known model can deal with yet. Thus, for a long bonded length, the definition of the E, E-S, E-S-D, S-D and D states that the interface undergoes until its failure is achieved with a single expression;
- The final branch of the load-slip curves is mainly changed only with the increase of the stiffness anchorage. So, with no end anchorage, a snap-back phenomenon can be seen as the loads decrease to zero with the increase of the interfacial slips. However, after the debonded load is reached and as the stiffness of the end anchorage increases, the snap-back phenomenon tends to be less obvious and after that, the loads tend to increase, once again, with the slips;
- An effective stiffness of the end anchorage could be identified, i.e., a stiffness beyond which the end anchorage can effectively improve the final strength of the mechanically anchored joint;
- When compared with the results obtained from the FEM, the proposed analytical approach had higher IAE values in the cases with the lowest stiffnesses of the end anchorage. If in the case of the longest bonded lengths the increase of the IAE value up to an approximate value of 20 % was attributed to the snap-back phenomenon that began at an earlier stage of the debonding process, in the case of the shortest bonded length, the IAE value of approximately 45 % was due to a slightly underestimation of the loads by proposed analytical approach. Nevertheless, for the other studied cases, the IAE values were approximately 1.0 %, which shows the high accuracy of this analytical approach with the FEM;
- The increase of the axial stiffness of FRP increases the debonded load but it does not have any influence of the spring, which failure will occur at the same ultimate slip. However, it demands the use of stiffer end anchorages so the ultimate load of the joint could be higher than the debonded load.

Despite being out of the scope of this work, the assumption of a nonlinear spring to define the load-slip behaviour of an end anchorage can be introduced into the proposed analytical approach once the relationship between the slips and the loads is known.

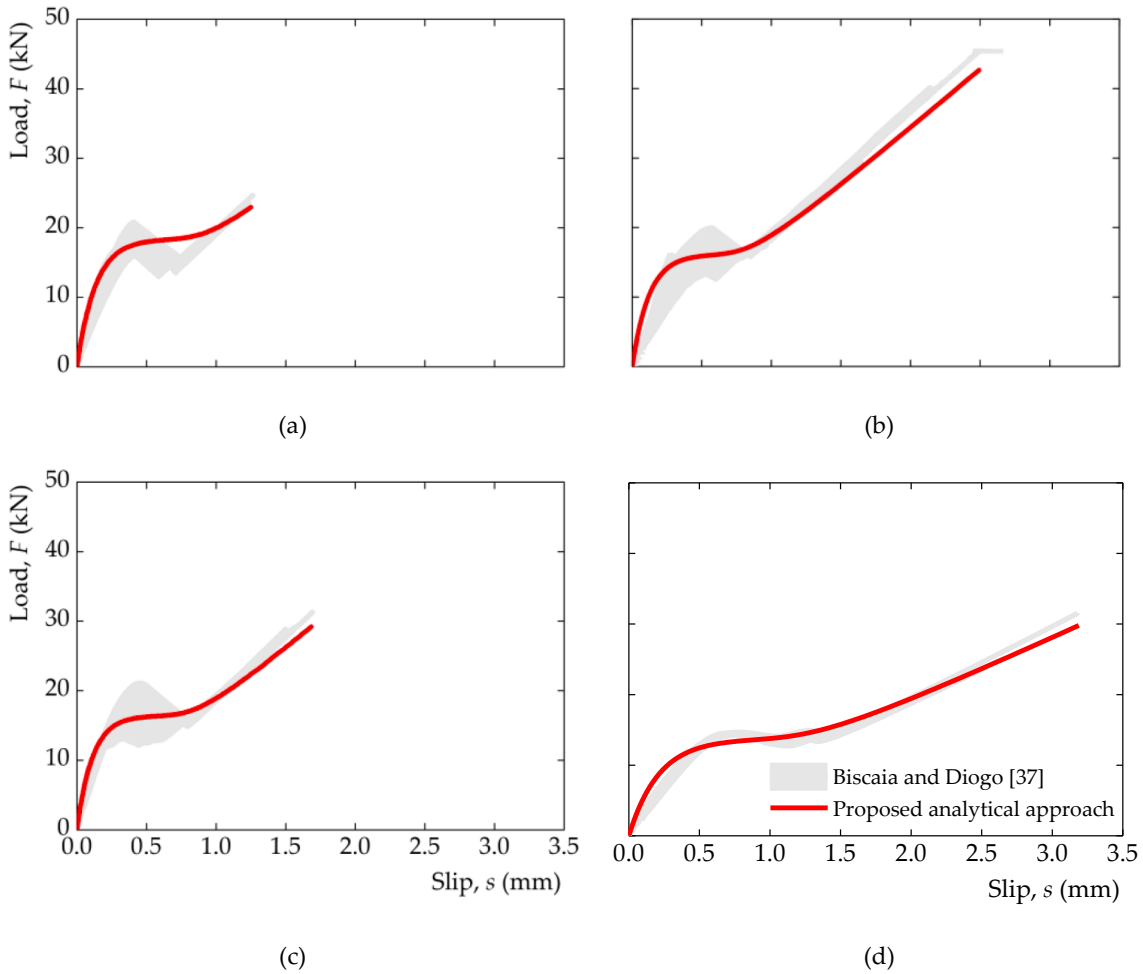

Fig. 17. Comparison between the experimental load-slip curve obtained by Biscaia and Diogo [37] and the load-slip curve predicted by the proposed analytical approach: (a) using a steel plate as end anchorage; (b) using two superposed L-shaped steel profiles as end anchorage; (c) using an embedded rectangular hollowed metallic profile as end anchorage; and (d) embedding the CFRP into the core of the timber as an end anchorage.

Therefore, this may open a new research topic in the understanding of other anchorage types such as the use of multiple adhesives, the influence of the adhesive or FRP thicknesses as well as any other commercial anchorage, through the same closed-form solution, which enlarges, even more, the applicability of the proposed analytical approach. For these reasons, the design-oriented equations herein proposed contributes for an worldwide use either for researchers or engineers acting in this area of knowledge.

CRediT authorship contribution statement

Hugo C. Biscaia: Writing – original draft, Validation, Software, Project administration, Methodology, Investigation, Funding acquisition, Formal analysis, Data curation, Conceptualization. **Jian-Guo Dai:** Writing – review & editing, Validation, Investigation.

Declaration of competing interest

The authors declare the following financial interests/personal relationships which may be considered as potential competing interests: Hugo C. Biscaia reports financial support was provided by Foundation for Science and Technology.

Jian-Guo Dai reports financial support was provided by City University of Hong Kong Startup Funding “Advanced Functional Construction Materials (AFCM) for Sustainable Built Environment” (Project code: 9380165).

Acknowledgments

The authors are thankful to Fundação para a Ciência e Tecnologia (FCT-MCTES) for the partial funding of this work under the strategic projects UIDP/00667/2020 and UIDB/00667/2020 and exploratory project EXPL/EME-APL/0994/2021 as well as City

University of Hong Kong Startup Funding “Advanced Functional Construction Materials (AFCM) for Sustainable Built Environment” (Project code: 9380165).

Data availability

Data will be made available on request.

References

[1] Ceroni F, Pecce M, Matthys S, Taerwe L. Debonding strength and anchorage devices for reinforced concrete elements strengthened with FRP sheets. Compos B Engng 2008;39(3):429–41.
[2] Wu YF, Huang Y. Hybrid bonding of FRP to reinforced concrete structures. J Compos Constr 2008;12(3):266–73.
[3] Zhang HW, Smith ST, Kim SJ. Optimisation of carbon and glass FRP anchor design. Constr Build Mater 2012;32:1–12.
[4] Zhang HW, Smith ST. Influence of FRP anchor fan configuration and dowel angle on anchoring FRP plates. Compos B Engng 2012;43(8):3516–27.
[5] Mostafa AAB, Razaqpur AG. A new CFRP anchor for preventing separation of externally bonded laminates from concrete. J Reinf Plast Compos 2013;32:1895–906.
[6] Mostafa A, Razaqpur AG. CFRP anchor for preventing premature debonding of externally bonded FRP laminates from concrete. J Compos Constr 2013;17:641–50.
[7] Biscaia HC, Micaelo R, Teixeira J, Chastre C. Numerical analysis of FRP anchorage zones with variable width. Compos B Engng 2014;67:410–26.
[8] Yang Y, Zhao J, Zhang S, Chastre C, Biscaia H. Effect of mechanical anchorage on the bond performance of double overlapped CFRP-to-steel joints. Compos Struct 2021;267:113902.
[9] Biscaia HC, Micaelo R. Emerging anchored FRP systems bonded to steel subjected to monotonic and cyclic loading: a numerical study. Engng Fract Mech 2022;261:108250.
[10] Zhang F, Gao L, Wei Q. Theoretical and numerical bonding capacity model of FRP-to-concrete joints with mechanical fastening. Constr Build Mater 2022;353:129066.
[11] Yuan H, Teng JG, Seracino R, Wu ZS, Yao J. Full-range behavior of FRP-to-concrete bonded joints. Engng Struct 2004;26(5):553–65.
[12] Dai JG, Ueda T, Sato Y. Development of the nonlinear bond stress-slip model of fiber reinforced plastics sheet-concrete interfaces with a simple method. J Compos Constr 2005;9(1):52–62.
[13] Mazzotti C, Savoia M, Ferracuti B. An experimental study on delamination of FRP plates bonded to concrete. Constr Build Mater 2008;22(7):1409–21.
[14] Fernando D, Yu T, Teng JG. Behavior of CFRP laminates bonded to a steel substrate using a ductile adhesive. J Compos Constr 2013;18(2):04013040.
[15] Biscaia HC, Chastre C, Viegas A. A new discrete method to model FRP–to-parent material bonded joints. Compos Struct 2015;121:280–95.
[16] Biscaia HC, Borba IS, Silva C, Chastre C. A nonlinear analytical model to predict the full-range debonding process of FRP-to-parent material interfaces free of any mechanical anchorage devices. Compos Struct 2016;138:52–63.
[17] Yuan C, Chen W, Pham TM. Bond behaviour between hybrid fiber reinforced polymer sheets and concrete. Construction and Building Materials 2019;210:93–110.
[18] Breña SF, McGuirk GN. Advances on the behavior characterization of FRP-anchored carbon fiber-reinforced polymer (CFRP) sheets used to strengthen concrete elements. Int J Concr Struct Mater 2013;7(1):3–16.
[19] Llauradó PV, Ibell T, Gómez JF, Ramos FJG. Pull-out and shear-strength models for FRP spike anchors. Compos B Engng 2017;116:239–52.
[20] Li W, Wei Liu Xu, Yang FX. Experimental study on FRP-to-concrete bonded joints with FRP sheet anchor system. Adv Mater Sci Engng 2020;2020:2514313.
[21] Sun W, Liu S, Zhang C. An effective improvement for enhancing the strength and feasibility of FRP spike anchors. Compos Struct 2020;247:112449.
[22] Alshami GS, Hawileh RA, Tatar J, Abdalla JA. Influence of CFRP spike anchors on the performance of flexural CFRP sheets externally bonded to concrete. J Compos Constr 2023;27(5).
[23] Biscaia H, Chastre C, Cruz D, Franco N. Flexural strengthening of old timber floors with laminated carbon fiber reinforced polymers. J Compos Constr 2017;20(1):04016073.
[24] Franco N, Chastre C, Biscaia H. Strengthening RC beams using stainless-steel Continuous Reinforcement Embedded at Ends. J Struct Engng 2020;146(5):04020065.
[25] Azevedo A, Firmo J, Correia J, Chastre C, Biscaia H, Franco N. Fire behaviour of CFRP-strengthened RC slabs using different techniques – EBR, NSM and CREatE. Compos B Engng 2022;230:109471.
[26] Narmashiri K, Jumaat MZ, Sulong NHR. Investigation on end anchoring of CFRP strengthened steel I-beams. Int J Phys Sci 2010;5(9):1360–71.
[27] Barris C, Correia L, Sena-Cruz J. Experimental study on the bond behaviour of a transversely compressed mechanical anchorage system for externally bonded reinforcement. Compos Struct 2018;200:217–28.
[28] Correia L, Barris C, França P, Sena-Cruz J. Effect of temperature on bond behavior of externally bonded FRP laminates with mechanical end anchorage. J Compos Constr 2019;23(5):04019036.
[29] Mazzotti C, Savoia M, Ferracuti B. A new single-shear set-up for stable debonding of FRP-concrete joints. Constr Build Mater 2009;23(4):1529–37.
[30] Biscaia HC, Chastre C, Silva C, Franco N. Mechanical response of anchored FRP bonded joints: a nonlinear analytical approach. Mech Adv Mater Struct 2018;25(3):238–52.
[31] Zhao S, Han J, Guo R, Feng X. Digital-image based performance analysis of CFRP–concrete interface bond under anchorage. Structures 2023;58:105345.
[32] Liu YL, Hong JQ, Deng J, Guo D, Dai JG. Structural performance of RC beams strengthened with hybrid bonded CFRP. J Build Eng 2024;88:109178.
[33] Hansen CS, Schmidt JW, Stan H. Transversely compressed bonded joints. Compos B Engng 2012;43(2):691–701.
[34] Biscaia HC, Chastre C, Silva MAG. Bond-slip model for FRP-to-concrete bonded joints under external compression. Compos B Engng 2015;80:246–59.
[35] Biscaia H, Chastre C. Design method and verification of steel plate anchorages for FRP-to-concrete bonded interfaces. Compos Struct 2018;192:52–66.
[36] Kalfat R, Smith ST. Anchorage devices used to improve the performance of reinforced concrete beams retrofitted with FRP composites: state-of-the-art review. J Compos Constr 2013;17:14–33.
[37] Biscaia H, Diogo P. Experimental analysis of different anchorage solutions for laminated carbon fiber-reinforced polymers adhesively bonded to timber. Compos Struct 2020;243:112228.
[38] Lu T, Li P, Cui C, Wu J, Fu B. Shear transferring mechanism of the FPR-to-concrete bonded joint with end U-jacketing: a theoretical study. Structures 2023;56:104991.
[39] Diab HM, Farghal OA. Bond strength and effective bond length of FRP sheets/plates bonded to concrete considering the type of adhesive layer. Compos B Engng 2014;58:618–24.
[40] Biscaia HC, Chastre C, Viegas A. A new discrete method to model unidirectional FRP-to-parent material bonded joints subjected to mechanical loads. Compos Struct 2015;121:280–95.
[41] Li A, Wang H, Li H, Kong D, Xu S. Estimation of bond strength and effective bond length for the double strap joint between carbon fiber reinforced polymer (CFRP) plate and corroded steel plate. Polymers 2022;14(15):3069.
[42] Silva CP. Comportamento de ligações adesivas entre compósitos de FRP e elementos estruturais de aço. MSc Thesis, NOVA School of Science and Technology, Universidade NOVA de Lisboa; 2015 [in Portuguese].
[43] Caggiano A, Martinelli E, Faella C. A fully-analytical approach for modelling the response of FRP plates bonded to a brittle substrate. Int J Solids Struct 2012;49(17):2291–300.

[44] Gao WY, Dai JG, Teng JG. Analysis of Mode II debonding behavior of fiber-reinforced polymer-to-substrate bonded joints subjected to combined thermal and mechanical loading. Engng Fract Mech 2015;136:241–64.
[45] Yang Y, Biscaia H, Chastre C, Silva MAG. Bond characteristics of CFRP-to-steel joints. J Constr Steel Res 2017;138:401–19.
[46] Nelson LA, Al-Allaf M, Weekes L. Analytical modelling of bond-slip failure between epoxy bonded FRP and concrete substrate. Compos Struct 2020;251:112596.
[47] Milani G, Grande E, Bertolesi E, Rotunno T, Fagone M. Debonding mechanism of FRP strengthened flat surfaces: analytical approach and closed form solution. Constr Build Mater 2021;302:124144.
[48] Biscaia HC, Chastre C, Borba IS, Silva C, Cruz D. Experimental evaluation of bonding between CFRP laminates and different structural materials. J Compos Constr 2016;20(3):04015070.
[49] He J, Xian G, Zhang YX. Numerical modelling of bond behaviour between steel and CFRP laminates with a ductile adhesive. Int J Adhes Adhes 2021;104:102753.
[50] Zhao J, Fang J, Yang Y, Zhang S, Biscaia H. Experimental study on mixed mode-I & II bond behavior of CFRP-to-steel joints with a ductile adhesive. Thin-Walled Struct 2023;184:110532.
[51] Biscaia H, Coelho P, Conde F, D'Antino T. Theoretical study on the bond performance of CFRP-to-steel single-lap shear tests with multiple debonding defects. Compos Struct 2024;345:118406.
[52] Zhou YU, Wu YF, Yun Y. Analytical modeling of the bond–slip relationship at FRP-concrete interfaces for adhesively-bonded joints. Compos B Engng 2010;41(6):423–33.
[53] Fawzia S, Zhao XL, Al-Mahaidi R. Bond-slip models for double strap joints strengthened by CFRP. Compos Struct 2010;92:2137–45.
[54] Dehghani E, Daneshjoo F, Aghakouchak AA, Khaji N. A new bond-slip model for adhesive in CFRP-steel composite systems. Engng Struct 2012;34:447–54.
[55] He J, Xian GJ. Debonding of CFRP-to-steel joints with CFRP delamination. Compos Struct 2016;153:12–20.
[56] Biscaia HC, Chastre C, Silva MAG. Analytical model with uncoupled adhesion laws for the bond failure prediction of curved FRP-concrete joints subjected to temperature. Theor Appl Fract Mech 2017;89:63–78.
[57] Wang HT, Wu G. Bond-slip models for CFRP plates externally bonded to steel substrates. Compos Struct 2018;184:1204–14.
[58] Biscaia H, Franco N, Chastre C. Development of a simple bond-slip model for joints monitored with the DIC technique. Arch Civ Mech Engng 2018;18(4):1535–46.
[59] Pang Y, Wu G, Wang H, Gao D, Zhang P. Bond-slip model of the CFRP-steel interface with the CFRP delamination failure. Compos Struct 2021;256:113015.
[60] Martinelli E. Closed-form solution procedure for simulating debonding in FRP strips glued to a generic substrate material. Fibers 2021;9(4):22.
[61] Nelson LA, Weekes L, Milani G, Al-Allaf M. Generalised analytical solutions for linear and non-linear bond-slip models for externally bonded FRP to a concrete substrate. Engng Struct 2024;298:117025.
[62] Zhao XL, Zhang L. State-of-the-art review on FRP strengthened steel structures. Engng Struct 2007;29(8):1808–23.
[63] Akbar I, Oehlers DJ, Ali MSM. Derivation of the bond–slip characteristics for FRP plated steel members. J Constr Steel Res 2010;66(8–9):1047–56.
[64] Fawzia S, Zhao XL, Al-Mahaidi R. Bond-slip models for double strap joints strengthened by CFRP. Compos Struct 2010;92(9):2137–45.
[65] Wang HT, Wu G, Dai YT, He XY. Determination of the bond–slip behavior of CFRP-to-steel bonded interfaces using digital image correlation. J Reinf Plast Compos 2016;35(18):1353–67.
[66] Doroudi Y, Fernando D, Zhou H, Nguyen VT, Ghafoori E. Fatigue behavior of FRP-to-steel bonded interface: an experimental study with a damage plasticity model. Int J Fatigue 2020;139:105785.
[67] Cornetti P, Muñoz-Reja M, Mantič V. Cohesive Crack Models and Finite Fracture Mechanics analytical solutions for FRP-concrete single-lap shear test: An overview. Theoretical and Applied Fracture Mechanics 2022;122:103529.
[68] Lu XZ, Teng JG, Ye LP, Jiang JJ. Bond-slip models for FRP sheets/plates bonded to concrete. Engineering Structures 2005;27(6):920–37.
[69] Biscaia HC. The influence of temperature variations on adhesively bonded structures: a non-linear theoretical perspective. Int J Non Linear Mech 2019;113:67–85.
[70] Biscaia HC, Canejo J, Zhang S, Almeida R. Using digital image correlation to evaluate the bond between carbon fibre-reinforced polymers and timber. Struct Health Monit 2021:1–24.
[71] Wu YF, Zhao XM. Unified bond stress-slip model for reinforced concrete. J Struct Engng 2013;139(11):1951–62.
[72] Shen D, Shi X, Ji Y, Yin F. Strain rate effect on bond stress-slip relationship between basalt fiber-reinforced polymer sheet and concrete. J Reinf Plast Compos 2015;34(7):547–63.
[73] Carvalho T, Chastre C, Biscaia H, Paula R. Flexural behaviour of RC T-beams strengthened with different FRP materials. Third International fib Congress Washington, May-June, 2010.
[74] Biscaia HC, Micaelo R, Chastre C. Cyclic performance of adhesively bonded joints using the Distinct Element Method: damage and parametric analysis. Compos B Engng 2019;178:107468.
[75] Biscaia HC, Micaelo R, Cornetti P, Almeida R. Numerical bond assessment of carbon-epoxy stepped-lap joints. Engng Fract Mech 2023;289:109413.
[76] Rozylo P, Falkowicz K. Stability and failure analysis of compressed thin-walled composite structures with central cut-out, using three advanced independent damage models. Compos Struct 2021;273:114298.
[77] Rozylo P, Debski H. Failure study of compressed thin-walled composite columns with top-hat cross-section. Thin-Walled Struct 2022;180:109869.
[78] Rozylo P. Comparison of failure for thin-walled composite columns. Materials 2022;15(1):167.
[79] Biscaia HC. Closed-form solutions for modelling the response of adhesively bonded joints under thermal loading through exponential softening laws. Mech Mater 2020;148:103527.
[80] Cervenka V, Jendele L, Cervenka J. ATENA Program Documentation – Part 1 – Theory. Prague: Cervenka Consulting; 2021.
[81] Biscaia HC, Chastre C, Silva MAG. Nonlinear numerical analysis of the debonding failure process of FRP-to-concrete interfaces. Compos B Engng 2013;50:210–23.
[82] Neubauer U, Rostásy FS. Design aspects of concrete structures strengthened with externally bonded CFRP-plates. In Proceedings of the 7th international conference on structural faults and repairs, vol. 2:109-118; 1997.
[83] Teng JG, Chen JF, Smith ST, Lam L. FRP strengthened RC structures. Chichester (England): John Wiley and Sons Ltd.; 2001.
[84] Fédération Internationale du Béton (FIB): bulletin d'information no. 14. Externally bonded FRP reinforcement for RC structures; July 2001.
[85] Ouezdou MB, Belarbi A, Bae SW. Effective bond length of FRP sheets externally bonded to concrete. Int J Concr Struct Mater 3(2):127–31.
[86] Fazli H, Yassin AYM, Shafiq N, Teo W. Effective bond length of CFRP sheets externally bonded to concrete beams under marine environment. Constr Build Mater 2018;167:726–38.
[87] Biscaia H, Chastre C. Theoretical analysis of fracture in double overlap bonded joints with FRP composites and thin steel plates. Engng Fract Mech 2018;190:435–60.
[88] Mostofinejad D, Arefian B. Generic assessment of effective bond length of FRP-concrete joint based on the initiation of debonding: Experimental and analytical investigation. Composite Structures 2021;277:114625.
[89] Popovics S. A numerical approach to the complete concrete stress-strain relation for concrete. Cem Concr Res 1973;3(5):583–99.